Princeton Plasma Physics Laboratory

PPPL-4046

PPPL-4046

Solution of Nonlinear Dispersive Partial Differential Equations using the Marker Method

Jerome L.V. Lewandowski

January 2005

Prepared for the U.S. Department of Energy under Contract DE-AC02-76CH03073.

PPPL Report Disclaimers

Full Legal Disclaimer

Trademark Disclaimer

PPPL Report Availability

This report is posted on the U.S. Department of Energy's Princeton Plasma Physics Laboratory Publications and Reports web site in Fiscal Year 2005. The home page for PPPL Reports and Publications is: http://www.pppl.gov/pub_report/

Office of Scientific and Technical Information (OSTI):

Available electronically at: http://www.osti.gov/bridge.

Available for a processing fee to U.S. Department of Energy and its contractors, in paper from:

U.S. Department of Energy
Office of Scientific and Technical Information
P.O. Box 62
Oak Ridge, TN 37831-0062

Telephone: (865) 576-8401

Fax: (865) 576-5728

E-mail: reports@adonis.osti.gov

National Technical Information Service (NTIS):

This report is available for sale to the general public from:

U.S. Department of Commerce
National Technical Information Service
5285 Port Royal Road
Springfield, VA 22161

Telephone: (800) 553-6847

Fax: (703) 605-6900

Email: orders@ntis.fedworld.gov

Online ordering: http://www.ntis.gov/ordering.htm

Modeling Solution of Nonlinear Dispersive Partial Differential Equations using the Marker Method

Jerome L. V. Lewandowski
Princeton University
Plasma Physics Laboratory,
Princeton, NJ 08543, USA

January 12, 2005

Abstract

A new method for the solution of nonlinear dispersive partial differential equations is described. The marker method relies on the definition of a convective field associated with the underlying partial differential equation; the information about the approximate solution is associated with the response of an ensemble of markers to this convective field. Some key aspects of the method, such as the selection of the shape function and the initial loading, are discussed in some details.

1 Introduction

Marker methods have been used for a long time in various disciplines (e.g. plasma physics, astrophysics, etc.) to give numerical solutions of purely convective problems [1, 2]. In these methods an ensemble of markers (or 'superparticles') is used to approximate the solution; the region of interest covered by the markers defines the phase space associated with the solution. Each marker is represented through its weight and position in phase space. The markers are advanced in time according to the characteristics ('equations of motion') of the underlying partial differential equation (PDE) associated with the problem. Marker methods are particularly useful for collisionless problems [1–4]. However, in many applications of interest (e.g. turbulent plasmas), diffusive processes can be important. Marker methods usually include diffusive effects in a perturbative fashion [5,6]: in the first step, the markers are evolved in phase space according to the collisionless (*i.e.* purely convective) dynamics; in the second step, diffusive effects are included by a randomization of the markers' weights and/or velocities according to a prescribed probability distribution. Although this method agrees with physical intuition, it is, from the numerical point of view, quite noisy and possibly inaccurate. The marker method presented in this paper allows for the *simultaneous* treatment of convective and diffusive effects.

The main idea behind the marker method for the solution of a given PDE is to rewrite it as a conservation equation with a generalized convective velocity. In general (even in linear cases), the generalized convective velocity depends on the solution of the PDE itself. Each marker, which carries the information of the solution of the PDE through its weight and its position, is advanced in time using a Lagrangian scheme. The generalized convective velocity mentioned earlier is computed through the information contained in the ensemble of markers and through the so-called shape function.

As it will become apparent in the next sections, the marker method can actually be applied to solve a general class of PDEs that are encountered commonly in physical and engineering sciences.

The marker method, unlike the finite difference and the finite element methods, does not rely on the concept of a grid (of course one can, if needed, reconstruct the solution on a fixed grid through the collective information associated with the markers). Increased resolution can be achieved in a natural way by locally increasing the number of markers and/or modifying the initial loading of the markers. Unlike the finite difference method, the marker method can be trivially extended to multi-dimensional problems.

This paper is organized as follows; in section 2, the marker method is described in the context of the solution of a one-dimensional linear diffusion equation. Some aspects of the marker method such as the shape function and the initial loading of the markers are also discussed in section 2 and numerical examples are provided. Numerical examples of the marker method for the linear diffusion equation, the nonlinear Burgers' equation, the Korteweg-de Vries equation and a highly-nonlinear diffusion equation are presented in section 3. Concluding remarks are given in section 4.

2 Marker Method

The purpose of this paper is to present a new numerical method for the solution of nonlinear dispersive PDEs, such as the nonlinear Burgers' equation [7–9]

$$\frac{\partial f}{\partial t} + f\frac{\partial f}{\partial x} = \mu\frac{\partial^2 f}{\partial x^2} \quad , \quad (\mu > 0) \tag{1}$$

and the Korteweg-de Vries (KdV) equation [10]

$$\frac{\partial f}{\partial t} + 3\frac{\partial f^2}{\partial x} + \frac{\partial^3 f}{\partial x^3} = 0 \, , \tag{2}$$

with initial conditions $f(x,0) = f_0(x)$. As mentioned in the Introduction, particle methods are usually applied to purely convective problems [*i.e.* by neglecting the right-hand side in Eq.(1)]. Therefore, the new aspect of the marker method is best described in the context of a simple example: the linear diffusion equation which is a limiting case of Eq.(1). An analysis of the smoothing approximation obtained through the shape function, which represents a crucial aspect of the method, is also discussed in this section. A specific numerical application of the marker method to the case of a one-dimensional linear diffusion equation is given.

2.1 Basic Idea

For illustrative purposes, we describe the marker method for one-dimensional problems (as mentioned in the Introduction, the generalization to multi-dimensional problems is straightforward). We consider an ensemble of N markers. Each marker k is defined through its position x_k and its weight W_k. The solution of a given one-dimensional PDE is found by allowing the set $\{(x_k, W_k); k = 1, \cdots, N\}$ to evolve in time according to a generalized nonlinear convective velocity. The generalized convective velocity usually depends on the solution itself and a form of convolution of the approximate solution with a shape function is required.

Consider the one-dimensional diffusion equation

$$\frac{\partial f}{\partial t} = \frac{\partial^2 f}{\partial x^2} \ , \tag{3}$$

subject to the initial condition $f_0(x) = f(x,0)$. The main idea behind the marker method is to write Eq.(3) as a conservation equation

$$\frac{\partial f}{\partial t} + \frac{\partial}{\partial x} (Vf) = 0 \ , \tag{4}$$

where

$$V = -\frac{1}{f} \frac{\partial f}{\partial x} \ . \tag{5}$$

For clarity, $f(x,t)$ is used to denote the exact solution of Eq.(3) whereas $F(x,t)$ represents its approximation. The function f can be approximated by an ensemble of markers (or 'superparticles') for which each marker j has an associated weight, W_j, and a time-dependent position, $x_j(t)$. As in standard particle methods, such an approximation can be written in terms of delta functions [1, 2]

$$\widehat{F} = \sum_{j=1}^{N} W_j \delta (x - x_j) \ , \tag{6}$$

where $\delta(x)$ is the usual Kronecker delta function; the hat notation indicates that the representation is singular. For example, $1/\widehat{F}(x,t)$ can be singular in region where $f(x,t)$ is nonzero; furthermore, the ratio of delta functions [implied in Eq.(5)] is not defined. Substituting the discrete representation (6) in Eq.(4) yields the characteristics associated with the generalized velocity V

$$\left.\begin{array}{rcl} dx_j/dt & = & V(x_j(t),t) \\ x_j(0) & = & x_{0j} \end{array}\right\} j = 1, \cdots, N \tag{7}$$

As noted above, $V \propto \partial\widehat{F}/\partial x/\widehat{F}$ is not well defined. As in conventional particle methods, a smoothed version of $\widehat{F}$ is obtained by taking the convolution of Eq.(6) with a shape function

$$F(x,t) = \left(S_\epsilon \star \widehat{F}\right)(x,t) = \sum_{j=1}^{N} W_j S_\epsilon (x - x_j) \ , \tag{8}$$

where $S_\epsilon(x) = S(x/\epsilon)/\epsilon$ and $\int S dx = 1$; ϵ is termed the support parameter. Using representation (8) in the trajectory equations, Eq.(7), one gets

$$\frac{dx_j}{dt} = -\frac{\sum_{k=1}^{N} W_k S'_\epsilon (x_j(t) - x_k(t))}{\sum_{k=1}^{N} W_k S_\epsilon (x_j(t) - x_k(t))} \ , \tag{9}$$

where a prime denotes a derivative with respect to x and the initial positions are $x_j(0) = x_{0j}$. Note that the weights in Eq.(9) do not vary in time; in particular, if all the weights are initially equal, then all the information about the approximation $F(x,t)$ is contained in the marker positions. The equations of motion (9) can be integrated using standard ordinary differential equation (ODE) techniques, such as the Runge-Kutta method [14], as used in this paper.

Before considering a numerical illustration of the marker method, several observations are in order. Clearly the accuracy of the marker method depends crucially on the shape function and its support parameter, ϵ (see next section). The number of markers, the method of integration of the equations of motion, the initial loading of the ensemble $\{(x_k, W_k); k = 1, \cdots, N\}$ and the time step of integration also do influence the accuracy of the marker method. In some sense, the positions of the markers define a moving grid as far as the approximate solution is concerned. Of course one can reconstruct the approximate solution F on a fixed grid $\{X_g; g = 1, \cdots, N_g\}$ at time t by invoking the representation (8):

$$F_g(t) \equiv F(X_g, t) = \sum_{j=1}^{N} W_j S_\epsilon(X_g - x_j(t)) \ .$$

The marker method can be easily generalized to *nonlinear* dispersive PDEs such as the KdV equation, Eq.(2), and Burgers' equation, Eq.(1). Both these equations can be written as conservation equations [Eq.(4)] with convective velocities

$$V(x,t) = 3f + \frac{1}{f} \frac{\partial^2 f}{\partial x^2} \ ,$$

for the KdV equation and

$$V(x,t) = \frac{f}{2} - \frac{\mu}{f} \frac{\partial f}{\partial x} \ ,$$

for Burgers' equation. The marker method is very versatile in its applications, whereas conventional (*e.g.* finite difference) methods usually require substantial modifications to account for additional nonlinear or dispersive terms, for example.

In summary, the marker method can be cast in the following algorithmic form;
1. initial stage:

- rewrite the original PDE as a conservation equation with generalized convective velocity V;
- select the number N of markers and the shape function S to approximate the solution; and
- load the markers according to a uniform or nonuniform spatial distribution.

2. main iteration loop:

- evaluate the (instantaneous) generalized convective velocity for each marker;
- integrate the characteristics (associated with the conservation equation) for a time step Δt.

The above algorithm (main iteration loop) is repeated N_t times, where N_t is a prescribed number of time steps.

The main differences between the marker method presented in this paper with conventional marker (PIC) methods are the following:

- The conventional PIC method is based on the original PDE whereas the present marker method is based on the equivalent conservation equation (associated with the original PDE).
- The conventional PIC method uses the splitting operator method to account for diffusive terms whereas the marker method treats convective and diffusive contributions simultaneously.

2.2 Analysis of the Smoothing Approximation

As mentioned in the previous section, the accuracy of the marker method depends crucially on the properties of the smoothed PDE's approximate solution. Therefore it is important to study the impact of the shape function and its support parameter ϵ on test functions. As it will become apparent below, the accuracy of the smoothing approximation is also related to the initial loading of the markers. The smoothed approximation of the exact solution $f(x)$ is given by

$$F(x) = \sum_{j=1}^{N} W_j S_\epsilon(x - x_j) \ , \tag{10}$$

where $S_\epsilon(x) = S(x/\epsilon)/\epsilon$ and the shape function $S(x)$ with finite support satisfies the normalization condition

$$\int_{-1}^{+1} S(x)dx = 1 \ ,$$

and $S(x) = 0$ for $|x| > 1$. In some cases, there are advantages in using shape functions with infinite support, in which case the normalization condition is of the form $\int_{-\infty}^{+\infty} Sdx = 1$. Apart from the actual form of the shape function, there is some freedom in selecting the value of the support parameter ϵ. However one can estimate an appropriate value for ϵ based on the following considerations. For illustrative purposes, consider a simulation with N markers that are initially distributed uniformly in the interval $x \in [-L, L]$; therefore, at $t = 0$, the average distance between markers is $h = 2L/N$. If the support parameter is such that $\epsilon < h$, then $S_\epsilon(x_j - x_k) \propto S((x_j - x_k)/\epsilon) = 0$ for all markers $j \neq k$; this implies that the position of each marker will be independent of the positions of the other markers at least at $t = 0$. We conclude that the support parameter must be larger than the average distance between markers, at least in the average sense. In addition, the value of ϵ, which is equivalent to a grid spacing in the finite difference method, must be chosen such as to accurately resolve the spatial scale length of $f(x)$. In summary, if λ denotes the (known or estimated) spatial scale length of $f(x)$ and h is the average distance between markers, the support parameter, ϵ, must satisfy the following inequality

$$h \ll \epsilon \ll \lambda \ .$$

There is some freedom in selecting a shape function. Typically one requires some smoothness properties and/or ease of computation (for example, a Gaussian shape function is smoother than a hat shape function, but it is computationally more demanding to evaluate). Below is a set of shape functions that are defined on the interval $[-1, +1]$:

$$\begin{aligned}
S_1(x) &= \frac{1}{2} \quad \text{(gate function)} \\
S_2(x) &= 1 - |x| \quad \text{(hat function)} \\
S_3(x) &= \frac{3}{4}\left(1 - x^2\right) \quad \text{(quadratic polynomial)} \\
S_4(x) &= \frac{15}{16}\left(1 - x^2\right)^2 \quad \text{(quartic polynomial)} \\
S_5(x) &= \mu\left(1 - |x|\right) e^{-x^2} \quad \text{(hat/Gaussian)} \\
S_6(x) &= \beta\left(1 - x^2\right)^2 e^{-x^2} \quad \text{(quartic polynomial/Gaussian)}
\end{aligned} \tag{11}$$

where $\mu = \left(\sqrt{\pi}\,\mathrm{erf}(1) + 1/e - 1\right)^{-1}$ and $\beta = 2/\left(\frac{3}{2}\,\mathrm{erf}(1) - 1/e\right)$ are constants of normalization, and $\mathrm{erf}(x)$ denotes the error function

$$\mathrm{erf}(x) = \frac{2}{\sqrt{\pi}} \int_0^x e^{-t^2} dt \ .$$

In some cases it is numerically convenient to use shape functions with infinite support such as, for example, the Gaussian shape function

$$S^{(0)}(x) = \frac{e^{-x^2}}{\sqrt{\pi}} \quad . \tag{12}$$

In order to improve the accuracy of an approximate solution $F = \left(S_\epsilon \star \widehat{F}\right)$ one can demand that some even moments of a Gaussian-based shape function vanish. If a shape function satisfies

$$\int_{-\infty}^{+\infty} x^{2q} S^{(N)}(x) dx = 0 \ ,$$

for $q = 1, \cdots, N$ then the smoothness of $S^{(N)}(x)$ is said to be order N. The systematic construction of shape functions with arbitrary smoothness order is described in Appendix A. The explicit expressions for $S^{(0)}$, $S^{(1)}$, $S^{(2)}$ and $S^{(3)}$ are

$$\begin{aligned}
S^{(0)}(x) &= \frac{e^{-x^2}}{\sqrt{\pi}} \ , \\
S^{(1)}(x) &= \left(\frac{3}{2} - x^2\right) \frac{e^{-x^2}}{\sqrt{\pi}} \ , \\
S^{(2)}(x) &= \left(\frac{15}{8} - \frac{5}{2}\, x^2 + \frac{1}{2}\, x^4\right) \frac{e^{-x^2}}{\sqrt{\pi}} \ , \\
S^{(3)}(x) &= \left(\frac{105}{48} - \frac{105}{24}\, x^2 + \frac{7}{4}\, x^4 - \frac{1}{6}\, x^6\right) \frac{e^{-x^2}}{\sqrt{\pi}} \ .
\end{aligned} \tag{13}$$

Note that the computational cost for evaluating $S_N(x)$ is dominated by the exponential factor e^{-x^2}. The shape functions given by Eqs.(13) are shown in Fig.1. In some applications, it can be advantageous to use shape functions with large N. In order to illustrate this point, we consider a positive-definite test function

$$\phi_M(x) = 1 + \sin\left(M\pi x/L\right) \ ,$$

defined in the interval $x \in [-L, L]$ and M is a positive integer (mode number). Fig.2 shows the approximate representation of $\phi_M(x)$ for shape functions with smoothness order 0,1,2,3 [Eq.(13) and Fig.1] for the mode number $M = 4$ and a set of $N = 32$ uniformly distributed markers. The exact test function is shown as a thick plain line. Clearly the approximation of $\phi_M(x)$ improves significantly as the smoothness order of the shape function is increased. Fig.3 shows the L^2 norm of the error for the test function $\phi_M(x)$ as a function of the mode number M for the shape functions of Eq.(13).

2.3 Initial Loading

The second factor that affects the approximation of $f(x)$ is the initial distribution of the position of the markers and their associated weights (referred to as the initial loading). There are two basic approaches to the initialization of the ensemble $\{(x_j, W_j)\ ;\ j = 1, \cdots, N\}$. In the first approach, the markers are uniformly distributed in space. Using the approximation of

$$\int f(x) dx \approx \sum_j f(x_j) h \ ,$$

where h is the distance between two consecutive markers, and noting that [see Eq.(6)]

$$\int \widehat{F} dx = \sum_j W_j \ ,$$

it follows that

$$\begin{aligned} W_j &= f(x_j)h \\ x_{j+1} - x_j &= h \ . \end{aligned}$$

In the second approach, each marker has the same weight, but the spatial distribution of the markers is not uniform. If there are N markers, the marker weight is then $W_j = \sigma/N$ where $\sigma \equiv \int_{-\infty}^{+\infty} f dx$. In order to determine the spatial distribution of the markers, it is convenient to introduce the variable

$$\xi = \frac{\int_{-\infty}^{x} f(x')dx'}{\int_{-\infty}^{+\infty} f(x')dx'} \ ,$$

which, by construction, is a positive-definite quantity in the unit interval. A uniform distribution in ξ, that is $\xi_j = (j - \frac{1}{2})/N$ $(\forall j)$, yields

$$\begin{aligned} x_j &= g^{-1}\left(\left(\int_{-\infty}^{+\infty} f(x)dx\right)\frac{j-\frac{1}{2}}{N}\right) \\ W_j &= \frac{\sigma}{N} \end{aligned} \tag{14}$$

where g^{-1} denotes the inverse of $g(x) \equiv \int_{-\infty}^{x} f(x')dx'$. As a numerical illustration, consider the function

$$f(x) = xe^{-x^2} \ ,$$

in the interval $x \in [0, x_0]$, $x_0 > 0$. The initialization based on a set of uniformly distributed x_j yields

$$\begin{aligned} x_j &= (j - 1/2)h \ , \\ W_j &= x_j e^{-x_j^2} h \ , \end{aligned}$$

where $h = x_0/N$. Alternatively, one can demand that each marker carries an equal weight; following the procedure described above [Eq.(14)] one obtains

$$\begin{aligned} x_j &= \sqrt{-\ln\left(1 - \frac{j-1/2}{N}\left(1 - e^{-x_0^2}\right)\right)} \\ W_j &= \frac{1}{N} \ , \end{aligned} \tag{15}$$

Fig.4 shows the smoothed approximation of $f(x)$ for a uniform spatial loading (dotted line) and a nonuniform spatial loading (dashed line) using a quadratic shape function with support parameter $\epsilon = 0.1$ for a set of $N = 32$ markers. The plain line represents the exact function. For the same parameters, the quartic shape function, which satisfies $S'(x = \pm 1) = 0$, yields a better approximation. Further improvement can be achieved using the shape function based on a quartic polynomial and a Gaussian function $[S(x) = S_6(x)$; see Eq.(11)]. Of course, smoother approximations can be obtained by increasing the number of markers N. Another parameter affecting the quality of the approximation is the support parameter, ϵ. Fig.5 shows the smoothed approximation of $f(x)$ for a uniform spatial loading (dotted line) and a nonuniform spatial loading (dashed line) using a quartic shape function with support parameter $\epsilon = 0.2$ for a set of $N = 32$

markers. Clearly a much better agreement between the approximated function and the exact function is found. If the support parameter is further increased the smoothing effect of $S(x)$ becomes too important and the quality of the approximated function degrades. This observation suggests the existence of an optimal support parameter; this is discussed in more detail in section 2.4.

2.4 Optimal Support Parameter

Consider a smooth, continuous function $f(x)$ on the interval $x \in [0, L]$. An approximation of $f(x)$ based on a set of N markers is written in the usual form of

$$F(x) = \sum_{j=1}^{N} W_j S_\epsilon(x - x_j) \ , \tag{16}$$

where $S_\epsilon(x) = S(x/\epsilon)/\epsilon$ denotes the shape function with argument x and support parameter ϵ. We assumed that the sequences associated with the marker positions $\{x_j; j = 1, \cdots, N\}$ and the marker weights $\{W_j; j = 1, \cdots, N\}$ are known. Note that if the support parameter ϵ is large then $F(x)$ will represent a smoothed version of $f(x)$ whereas a too small value of ϵ may generate a spurious oscillatory behavior in $F(x)$. Intuitively there should exist an optimal value of the support parameter, $\epsilon_{\rm opt}$. In order to determine $\epsilon_{\rm opt}$, we use a quadratic optimization technique. We define a positive-definite energy functional

$$E = \sum_{g=1}^{N} \left(F(X_g) - f(X_g)\right)^2 \tag{17}$$

based on a uniform grid $X_g = (g - 1/2)\Delta X$ and $\Delta X = L/N_g$ is the grid spacing. We assume that the support parameter depends on a (continuous) time-like coordinate τ: $\epsilon = \epsilon(\tau)$. The dynamical equation governing the support parameter is

$$\frac{d\epsilon}{d\tau} = -\frac{\partial E}{\partial \epsilon} \ . \tag{18}$$

In the limit $\tau \mapsto \infty$, we expect $\epsilon \mapsto \epsilon_{\rm opt}$. Using Eqs.(16,17) the explicit form of Eq.(18) is

$$\frac{d\epsilon}{d\tau} = \frac{2}{\epsilon^2} \sum_{k=1}^{N_g} \left(F(X_k) - f(X_k)\right) \Theta_k \ , \tag{19}$$

where

$$\Theta_k \equiv \sum_{j=1}^{N} W_j \left(S(z_{jk}) + z_{jk} S'(z_{jk})\right) \ , \tag{20}$$

$z_{jk} \equiv (X_k - x_j)/\epsilon$ and a prime denotes a derivative with respect to the argument. We note that the right-hand side of Eq.(19) depends nonlinearly on ϵ through $F(X_k)$, z_{jk} and the factor $1/\epsilon^2$ that multiplies the summation. Eq.(19) can be advanced in time using standard ODE integrators. We now consider a numerical example using a superGaussian with finite support

$$S(x) = C\left(1 - x^2\right) e^{-x^2} \ ,$$

where $C = (1/e + \sqrt{\pi}\,\mathrm{erf}(1)/2)^{-1}$ is a constant of normalization and as before $\mathrm{erf}(x)$ denotes the error function. Eq.(19) has been integrated using a fourth-order Runge-Kutta scheme. The

dotted line in Fig.6 shows the approximated profile, $F(x)$ using the optimal parameter $\epsilon_{\rm opt} = 0.0213$ for the function

$$f(x) = 3A\mathrm{sech}^2(\beta(x-1)) \; , \tag{21}$$

with parameters $A = 0.3$, $\beta = \sqrt{A/4\alpha}$ and $\alpha = 0.000484$. The dashed line represents $F(x)$ for the initial value of $\epsilon(0) = 1.0$ whereas $f(x)$ is show as a thin plain line. The number of grid points is $N_g = 100$, the number of markers is $N = 400$ and the time step is $\Delta\tau = 0.05$. The fast convergence of the quadratic optimization algorithm is due to the factor $1/\epsilon^2$ in Eq.(19). The quadratic optimization algorithm has been tested for various functions $f(x)$; in all cases the approximated profile $F(x)$ at $\epsilon = \epsilon_{\rm opt}$ was in excellent agreement with the exact profile $f(x)$, indicating that the algorithm is robust and reliable.

3 Numerical Examples

The purpose of this section is to illustrate the marker method for the linear diffusion equation (section 3.1), the nonlinear Burgers' equation (section 3.2), the Korteweg-de Vries equation (section 3.3) and a highly nonlinear diffusion equation (section 3.4).

3.1 Linear Diffusion Equation

In this section, we apply the marker method for the diffusion equation, Eq.(3), with initial conditions

$$\left.\begin{array}{rcl} f_0(x) & = & 1 \; ; \; |x| \le 1 \\ & = & 0 \; ; \; |x| > 1 \end{array}\right\} \tag{22}$$

The solution of the diffusion equation, Eq.(3), with initial conditions (22) is easily found using Laplace transforms

$$\begin{aligned} f(x,t) &= \frac{1}{\sqrt{4\pi t}} \int_{-\infty}^{+\infty} f_0(\xi) \exp\left(-(x-\xi)^2/4t\right) d\xi \\ &= \frac{1}{2} \left[\mathrm{erf}\left(\frac{x+1}{2\sqrt{t}}\right) - \mathrm{erf}\left(\frac{x-1}{2\sqrt{t}}\right) \right] \; , \end{aligned}$$

where, as before, $\mathrm{erf}(x)$ is the error function with argument x. As mentioned in the previous section, there is some freedom in the choice of the shape function $S(x)$. Here we consider a shape function with infinite support [see Eq.(13)]

$$S^{(1)}(x) = \frac{3/2 - x^2}{\sqrt{\pi}} \; e^{-x^2} \; . \tag{23}$$

The equations of motion (9) have been integrated using a second-order Runge-Kutta method with a fixed time step. The approximate solution has been reconstructed on a moving grid defined by the marker positions $\mathbf{x}(t) = \{x_j(t); j = 1, \cdots, N\}$. Note that one can determine the approximate solution on a fixed, prescribed grid; however this approach involves the shape function (or some other form of interpolation) that further reduces the accuracy of the numerical scheme. Fig.7 shows the exact solutions (plain line: $t = 2.0$; dotted line: $t = 4.0$) and the approximate solutions (triangles: $t = 2.0$; squares: $t = 4.0$) of the diffusion equation for a set of $N = 100$ markers. The initial condition is the square profile of Eq.(22). The parameters are: $\Delta t = 0.01$, $\epsilon = 1/3$ and $L = 14.0$. We note the excellent agreement of the approximate solution with the exact solutions. As it can be expected, slight errors do appear when $F \mapsto 0$ although their magnitude are small.

Although not shown here, we have noted that the use of certain shape functions with finite support can sometime lead to a clustering effect in the marker position, that is the solution appears to display an additional scale length associated with the support parameter. In general, the use of shape function with infinite support appear to improve the accuracy of the approximate solution.

3.2 Nonlinear Burgers' Equation

As a second example, we apply the marker method to the solution of the nonlinear Burgers' equation. Following the methodology presented in Section 2.1, the nonlinear Burgers equation can be written as a conservation equation

$$\frac{\partial f}{\partial t} + \frac{\partial}{\partial x}\ (Vf) = 0\ ,$$

where

$$V = \frac{f}{2} - \frac{\mu}{f}\ \frac{\partial f}{\partial x}\ . \tag{24}$$

It is interesting to note that the nonlinear term in Burgers' equation appears as a linear term in the convective velocity [first term in Eq.(24)] whereas the linear term in Eq.(1), which accounts for the diffusive process, is represented as a nonlinear term in f [second term in Eq.(24)]. Before presenting numerical results pertaining to the full nonlinear Burgers' equation, we consider the 'wave breaking' effect associated with the quasilinear case [$\mu = 0$ in Eq.(1)]

$$\frac{\partial f}{\partial t} + f\frac{\partial f}{\partial x} = 0\ , \tag{25}$$

with initial condition $f(x,0) = f_0(x)$. The presence of the diffusive term in the original Burgers' equation prevents the solution from becoming multiple valued. The exact solution of Eq.(25) is

$$f(x,t) = f_0(x - ft)\ . \tag{26}$$

The explicit solution of Eq.(26) for f amounts to a root finding problem. In this paper the bisection method [14] has been used to solve Eq.(26). In the present case, the initial condition was chosen as $f_0(x) = \mathrm{sech}^2 x$. The solution of the quasilinear problem (25) provides a simple theoretical description of a shock wave. The time at which the shock forms may be estimated by identifying it with the earliest time, t_c, at which the profile $f(x,t)$ becomes vertical, that is, the time at which $\partial f/\partial x = \infty$ for some point on the curve. From Eq.(26) we have the general relation

$$\partial f/\partial x = \frac{f_0'}{1 + tf_0'}\ ,$$

where a prime denotes a differentiation with respect to the argument. For the specific initial profile of $f_0(x) = \mathrm{sech}^2 x$, we have $f_0'(x) = -2\mathrm{sech}^2 x \tanh x$. On using the largest negative value of this expression (namely $x_c = -4\sqrt{3}/9$) to obtain the earliest time, we find $t_c = 1.299$. Fig.8 shows the the initial profile (thick plain line) and the exact solutions at $t = 0.4, 0.8, 1.2$ are shown by thin plain lines. The symbols represents the approximate solutions based on the markers' positions. We note that the marker method is able to capture the transition just before the wave breaking phenomenon very accurately; the algorithm fails around $t \simeq 1.3$ in good agreement with our estimate for the critical time t_c. We would like to point out that the complexity of the algorithm for this *nonlinear* quasilinear problem is the same as that of the *linear* diffusion equation discussed in the previous section. This is in contrast with finite difference methods

for which the linear diffusion equation and the nonlinear quasilinear problem (25) would require different algorithms.

Having considered the limit cases of Eq.(1), we now present a numerical example for the full nonlinear Burgers' equation. Given the initial profile of

$$f_0(x) = f(x,0) = \frac{\mu}{\lambda}\ \left(A - 4\tanh(x/\lambda)\right)\ ,$$

where μ, A and λ are constants, the exact solution of Burgers's equation is (see Appendix B)

$$f(x,t) = 2\mu\ \frac{2a\ e^{\mu t a^2 - ax} + b\ e^{\mu t b^2 - bx} + c\ e^{\mu t c^2 - cx}}{2\ e^{\mu t a^2 - ax} + e^{\mu t b^2 - bx} + e^{\mu t c^2 - cx}}\ \ , \tag{27}$$

where $a = A/2\lambda$, $b = a + 2/\lambda$ and $c = a - 2/\lambda$. Fig.9 shows the exact (thin plain lines) and approximate (symbols) solutions at $t = 0$, $t = 100$ and $t = 200$. The simulation has been carried out with $N = 256$ markers (with an initial uniform spatial distribution) and a time step of integration $\Delta t = 0.1$. Other parameters are: $A = 4.0$, $\lambda = 7.0$ and $\mu = 0.1$. We note that the marker method is able to capture the steepening of the front with a very good accuracy.

3.3 Korteweg-de Vries Equation

In this section, the marker method is applied to the Korteweg-de Vries equation, Eq.(2). This equation has been found relevant in various physical models such as shallow water waves [10], ion acoustic waves in plasmas [12] and acoustic waves in an anharmonic crystal [13] and other applications [11]. As before, Eq.(2) can be written as a conservation equation, Eq.(4), with convective velocity

$$V(x,t) = 3f(x,t) + \frac{1}{f}\ \frac{\partial^2 f(x,t)}{\partial x^2}\ \ . \tag{28}$$

The equations of motion are given by

$$\begin{aligned} \frac{dx_k}{dt} &= V(x_k,t)\ , \\ x_k(0) &= x_{0k} \end{aligned} \tag{29}$$

where

$$V(x_k,t) = 3\sum_{j=1}^{N} W_j S_\epsilon(x_k - x_j) + \frac{\sum\limits_{j=1}^{N} W_j S''_\epsilon(x_k - x_j)}{\sum\limits_{j=1}^{N} W_j S_\epsilon(x_k - x_j)}\ \ .$$

The simulations reported here were carried out using 2 different shape functions. The first shape function has finite support (here defined in the interval $x \in [-1,1]$) and it given by

$$S_6(x) = \beta\left(1 - x^2\right)^2 e^{-x^2}\ , \tag{30}$$

where $\beta = 2/\left(\frac{3}{2}\ \mathrm{erf}(1) - 1/e\right)$. The second shape function is a superGaussian with infinite support [see Eq.(13)]

$$S^{(1)}(x) = \frac{1}{\sqrt{\pi}}\ \left(\frac{3}{2}\ - x^2\right) e^{-x^2}\ . \tag{31}$$

The accuracy of the marker method depends in part on the choice of the support parameter. If the average distance between markers at $t = 0$ is denoted h, the support parameter can be chosen of the form $\epsilon = \alpha\sqrt{h}$ where α is a free parameter. If α is too small, the representation of f will be 'noisy' (oscillatory) and the error norm will be large. If, however, α is large, then the reconstructed function $F(x,t)$ will represent a smoothed version of the actual profile $f(x,t)$ and therefore the error norm will be large. Fig.10 shows the L^2 norm of the error computed on a fixed grid with $N_g = 5000$ points for the profile $f_0(x) = \mathrm{sech}^2(x/2)/2$ as a function of the parameter α. The number of markers is $N = 128$ uniformly distributed in the interval $x \in [-L, L]$ where $L = 12$ (the distance between markers is then $h = 2L/N$). As expected the error norm drops with α for small α but increases with α for $\alpha \sim 1$. A value of $\alpha = 0.5$ appears to be optimal for this particular profile and number of markers. Fig.11 shows the initial profile (dotted line)

$$f(x,0) = f_0(x) = \frac{1}{2}\,\mathrm{sech}^2(x/2)\;, \tag{32}$$

for a set of $N = 128$ markers, each marker having the same weight. The triangles represent the position of the markers. The solution of Eq.(2) for the initial profile (32) is the soliton given by

$$f(x,t) = \frac{1}{2}\,\mathrm{sech}^2((x-t)/2)\;.$$

Fig.12 shows the exact solution of Eq.(2) with initial conditions (32) at $t = 1.0$ (dotted line). The triangles represent the position of the markers ($N = 128$). Each marker has the same weight, the time step is $\Delta t = 0.002$ and the shape function used is the superGaussian, Eq.(31). Clearly the algorithm fails to capture the correct solution as the markers tend to 'coalesce' in the vicinity of the maxima of F. The numerical solution does not even resemble the exact solution if one uses a shape function with finite support [Eq.(30)] as shown in Fig.13 (other parameters are the same as in Fig.12). Fig.12 and Fig.13 were obtained by loading the markers nonuniformly in space such that $W_k = \text{const}$. An alternative is to load the markers uniformly in space resulting in nonuniform weights. Fig.14 represents the numerical solution of Eq.(29) with the same parameters as in Fig.12 for a uniform loading in x. The positions of the markers (triangles) are in excellent agreement with the exact solution (shown as a dotted line). If one uses a larger timestep, $\Delta t = 0.01$, one notices (Fig.15) the formation of a front around $x = 3$. The marker method has also been tested for the case of a two-soliton problem. Given the initial condition of

$$f_0(x) = 6\,\mathrm{sech}^2 x\;, \tag{33}$$

the solution of the KdV equation is [11]

$$f(x,t) = 12\,\frac{3 + 4\cosh(2x - 8t) + \cosh(4x - 64t)}{\left(3\cosh(x - 28t) + \cosh(3x - 36t)\right)^2}\quad . \tag{34}$$

Fig.16 shows the numerical solution (triangles) and the exact solution (dotted line) at $t = 0.05$ for the initial conditions of Eq.(33). The number of markers used is $N = 500$, the time step is $\Delta t = 10^{-5}$ and the support parameter is $\epsilon = \sqrt{h}$. We note the excellent agreement between the numerical solution and the exact solution. In the general case when the exact solution is not known, one must carry out a scan in the time step (the final solution must be independent of the time step). Fig.17 shows the L^2 norm of the error measured at $t = 0.1$ for the case of Fig.16 as a function of the time step. As expected a large step yields an inaccurate solution. The error norm becomes independent of the time step for $\Delta t < 0.0014$.

3.4 Nonlinear Diffusion Equation

In this section, we apply the marker method to the solution of nonlinear diffusion equations. As in the previous section, we consider the one-dimensional case as the complexity of the algorithm

is not affected by the dimensionality of the problem. The nonlinear diffusion equation is written

$$\frac{\partial f}{\partial t} = \frac{\partial}{\partial x}\left(D\frac{\partial f}{\partial x}\right) + Q(x) \ , \tag{35}$$

with a diffusion coefficient of the form $D = D_0 f e^{-f}$ and a source term

$$Q(x) = -D_0 e^{-f_\infty}\left[f_\infty \frac{\partial^2 f_\infty}{\partial x^2} + (1-f_\infty)\left(\frac{\partial f_\infty}{\partial x}\right)^2\right] \ . \tag{36}$$

Here $f_\infty = f_\infty(x)$ denotes the steady state solution of Eq.(35). The nonlinear diffusion equation (35) can be written as a conservation equation [Eq.(4)] with a generalized convective velocity given by

$$V(x,t) = -\frac{D\partial f/\partial x + S(x)}{f} \ , \tag{37}$$

where

$$S(x) = \int_{-\infty}^{x} Q(x')dx' \ . \tag{38}$$

The presence of the integral in Eq.(38) can be computationally prohibitive since $S(x)$ is required for every marker at every time step. In order to bypass this difficulty, $S(x)$ has been computed at the beginning of the simulations for a set of fixed grid points; the evaluation of this quantity at the marker position is carried out through a linear interpolation using tabulated values of $S(x)$.

The steady state solution has been taken as

$$f_\infty(x) = \exp\left(-\alpha(x+x_0)^2\right) + \exp\left(-\alpha(x-x_0)^2\right) \ , \tag{39}$$

and the initial profile is a Gaussian centered at $x = 0$:

$$f_0(x) = f(x,0) = e^{-x^2} \ . \tag{40}$$

Fig.18 shows the steady state solution [Eq.(39)] and the initial profile (triangles) for a set of $N = 256$ markers uniformly distributed in the interval $[-5/2, 5/2]$. Other parameters are $\alpha = 4.0$, $x_0 = 0.5$ and $D_0 = 10$; the support parameter has been chosen as $\epsilon = \sqrt{h}$ where h is the average distance between markers at $t = 0$. As in the linear case, the equations of motion have been advanced in time using a second-order Runge-Kutta integrator [14] with a fixed time step $\Delta t = 0.01$. Fig.19 shows the steady solution and the approximate solution at the marker positions (triangles) at $t = 80$. We note the excellent agreement between the computed solution and the exact solution. This numerical example highlights one important advantage of the marker method: it is accurate in determining the long-time behavior of highly nonlinear dispersive equations. Further the actual implementation of the algorithm is straightforward and be easily adapted to more complex nonlinear dispersive PDEs.

4 Conclusions

In this paper we have introduced the marker method for the solution of the nonlinear dispersive partial differential equations. The main idea behind the marker method is to rewrite a given PDE as a conservation equation. A set of markers is then advanced in time (Lagrangian scheme) according to a generalized convective velocity associated with the conservation equation [which

itself is an alternative (but exact) form of the original PDE]. The information about the approximate solution can be obtained through a convolution of the markers' weights and positions with a shape function.

In this paper, we have addressed several aspects of the marker method such as the choice of the shape function and the initial loading of the markers. Numerical examples have demonstrated that the marker method yields accurate solutions for the linear and nonlinear diffusion equation, the nonlinear Burgers' equation and the Korteweg-de Vries equations.

The main advantages of the marker method are its ease of implementation, flexibility and accuracy. Further, the marker method is naturally applicable to PDEs which solutions display one or more shocks since the method is Lagrangian in nature; finite difference methods are often (but not always) not accurate in such situations. The accuracy of the marker method is dependent on the number of markers and the specific shape function used. Although shape functions with finite support are usually 'cheaper' to evaluate, they can sometimes lead to a clustering effect with the number of markers is insufficient. Numerical results have confirmed that shape functions with infinite support are usually (but not always) preferable. The number of markers N affects the accuracy of the solution in a more direct way. The quantity $2L/N$ (where $2L$ is the typical spatial extent of the domain of interest in the one-dimensional case) can be seen as the analogue of a grid spacing in the finite-difference method. Clearly an increase in the number of markers yields a more accurate solution.

The solution of integral equations using the marker method is more difficult and will be addressed in future publications.

Acknowledgments

This research was supported by Contract No DE-AC02-76CH03073 and the Scientific Discovery through Advanced Computing (SciDAC) initiative (U.S. Department of Energy).

References

[1] C.K. Birsdall and A.B. Langdon, *Plasma Physics via Computer Simulations*, McGraw-Hill, New York (1985).

[2] R.W. Hockney and J.W. Eastwood, *Computer Simulations using Particles*, McGraw-Hill, New York (1981).

[3] J.L.V. Lewandowski, Phys. of Plasmas, **10**, 3204 (2003).

[4] J.L.V. Lewandowski, J. of Scientific Computing , **21**(2), 174 (2004).

[5] R. Shanny, J.M. Dawson and J.M. Greene, Phys. Fluids, **10**, 1281 (1967).

[6] J.L.V. Lewandowski, Can. J. Phys., **81**, 1331 (2003).

[7] J.M. Burgers, *The Nonlinear Diffusion Equation: Asymptotic Solutions and Statistical Problems*, Reidel, Boston (1977).

[8] J.D. Cole, Quart. Appl. Math. **9**, 225 (1951).

[9] E. Hopf, Comm. Pure Appl. Math. **3**, 201 (1950).

[10] D.J. Korteweg and G. de Vries, Philos. Mag. **39**, 422 (1895).

[11] P.G. Drazin and R.S. Johnson, *Solitons: An Introduction*, Cambridge University Press, Cambridge (1989).

[12] E. Infeld and G. Rowlands, *Nonlinear Waves, Solitons and Chaos*, Cambridge University Press, Cambridge (2000).

[13] W.F. Ames, *Nonlinear Partial Differential Equations*, Academic Press, New York (1967).

[14] W.S Press, S.A. Teukolsky, W.T. Vetterling and B.P. Flannery, *Numerical Recipes in Fortran*, Cambridge University Press, New York (1992).

Appendix A: Construction of Shape Functions

We consider shape functions of the form

$$S(x) = p_N(x)h(x) \; , \tag{41}$$

where $p_N(x)$ is a polynomial of order $2N$

$$p_N(x) = \sum_{n=0}^{N} \alpha_n x^{2n} \; . \tag{42}$$

and $h(x) = e^{-x^2}/\sqrt{\pi}$ is a normalized Gaussian. The shape function must satisfy the normalization constraint of

$$\int_{-\infty}^{+\infty} S(x)dx = 1 \; . \tag{43}$$

We may also require that additional (even) moments of S vanish. A shape function with smoothness order N is defined such that $S(x)$ satisfies the constraint

$$\int_{-\infty}^{+\infty} x^{2q} S(x)dx = 0 \; , \tag{44}$$

for $q = 1, \cdots, N$ as well as the normalization constraint, Eq.(43). The system (43,44) has $N+1$ equations for $N+1$ unknown coefficients $\alpha_0, \alpha_1, \cdots, \alpha_N$. The equations to be solved are

$$\left.\begin{array}{rcll} \sum\limits_{n=0}^{N} \alpha_n I_n & = & 1 \; , & \\ \sum\limits_{n=0}^{N} \alpha_n I_{n+q} & = & 0 \; , & q = 1, \cdots, N \end{array}\right\} \tag{45}$$

where

$$I_n \equiv \frac{1}{\sqrt{\pi}} \int_{-\infty}^{+\infty} x^{2n} e^{-x^2} dx = \frac{(2n-1)(2n-3)(2n-5)\cdots(5)(3)(1)}{2^n} \equiv \frac{(2n-1)!!}{2^n} \quad ,$$

for $n = 1, 2, \cdots$ and $I_0 = 1$. The solution of system (45) is

$$\boldsymbol{\alpha} = A^{-1}\mathbf{u} \; ,$$

where $\boldsymbol{\alpha} = (\alpha_0, \alpha_1, \cdots, \alpha_{N-1}, \alpha_N)^T$, $\mathbf{u} = (1, 0, \cdots, 0)^T$ are column vectors with $N+1$ elements and

$$A = \begin{pmatrix} I_0 & I_1 & I_2 & \cdots & I_N \\ I_1 & I_2 & I_3 & \cdots & I_{N+1} \\ I_2 & I_3 & I_4 & \cdots & I_{N+2} \\ \cdots & \cdots & \cdots & \cdots & \cdots \\ I_{N-1} & I_N & I_{N+1} & \cdots & I_{2N-1} \\ I_N & I_{N+1} & I_{N+2} & \cdots & I_{2N} \end{pmatrix} \; .$$

The explicit expressions for the shape functions with smoothness order $N = 0$ to $N = 3$ are

$$
\begin{aligned}
S^{(0)}(x) &= \frac{e^{-x^2}}{\sqrt{\pi}} \ , \\
S^{(1)}(x) &= \left(\frac{3}{2} - x^2 \right) \frac{e^{-x^2}}{\sqrt{\pi}} \ , \\
S^{(2)}(x) &= \left(\frac{15}{8} - \frac{5}{2}\, x^2 + \frac{1}{2}\, x^4 \right) \frac{e^{-x^2}}{\sqrt{\pi}} \ , \\
S^{(3)}(x) &= \left(\frac{105}{48} - \frac{105}{24}\, x^2 + \frac{7}{4}\, x^4 - \frac{1}{6}\, x^6 \right) \frac{e^{-x^2}}{\sqrt{\pi}} \ .
\end{aligned}
$$

Appendix B: Analytical Solution of Burgers' Equation

The nonlinear Burgers' equation is

$$\frac{\partial f}{\partial t} + f\frac{\partial f}{\partial x} = \mu\frac{\partial^2 f}{\partial x^2} \ , \tag{46}$$

where $\mu > 0$ is the diffusion coefficient. It is easy to show that the function

$$\theta(x,t) = \exp\left(-\frac{1}{2\mu}\int f(x,t)dx\right) \ ,$$

satisfies the diffusion equation

$$\frac{\partial \theta}{\partial t} = \mu\frac{\partial^2 \theta}{\partial x^2} \ . \tag{47}$$

Therefore a simple prescription for solving Burgers' equation, Eq.(46), is (given an initial profile $f_0(x) = f(x,0)$)

- determine $\theta(x,0) = \exp\left(-\int f_0(x)dx/2\mu\right)$;
- obtain $\theta(x,t)$ by solving the diffusion equation (47); and
- determine $f(x,t)$ from $f(x,t) = -2\mu\partial\theta/\partial x/\theta$.

Consider the following initial profile

$$f_0(x) = f(x,0) = \frac{\mu}{\lambda}\ (A - 4\tanh(x/\lambda)) \ .$$

Using the relation of $\int \tanh x dx = \ln(\cosh x) + C$, we obtain

$$\theta(x,0) = \widehat{\theta}\exp(-Ax/2\lambda)\cosh^2(x/\lambda) \ , \tag{48}$$

where $\widehat{\theta} = \exp(Ax_0/2\lambda)\mathrm{sech}^2(x_0/\lambda)$ and x_0 are constants. The solution of the diffusion equation, Eq.(47), is

$$\theta(x,t) = \int_{-\infty}^{+\infty} G(\xi,x,t)\theta(\xi,0)d\xi \ ,$$

where

$$G(\xi,x,t) = \frac{1}{\sqrt{4\pi\mu t}}\ \exp\left(-\frac{(x-\xi)^2}{4\mu t}\ \right)$$

is the Green's function. After some algebra one obtains

$$\theta(x,t) = \frac{\widehat{\theta}}{4}\ \left(2\ e^{\mu t a^2 - ax} + e^{\mu t b^2 - bx} + e^{\mu t c^2 - cx}\right) \ ,$$

where $a = A/2\lambda$, $b = a + 2/\lambda$ and $c = a - 2/\lambda$ and

$$\begin{aligned} f(x,t) &= -\frac{2\mu}{\theta(x,t)}\ \frac{\partial\theta}{\partial x} \\ &= 2\mu\ \frac{2a\ e^{\mu t a^2 - ax} + b\ e^{\mu t b^2 - bx} + c\ e^{\mu t c^2 - cx}}{2\ e^{\mu t a^2 - ax} + e^{\mu t b^2 - bx} + e^{\mu t c^2 - cx}} \ . \end{aligned} \tag{49}$$

For the special case $A = 0$ (see Eq.(48)), Eq.(49) simplifies to

$$f(x,t) = -\frac{4\mu}{\lambda}\ \frac{\sinh(2x/\lambda)}{\cosh(2x/\lambda) + e^{-4\mu t/\lambda^2}} \ .$$

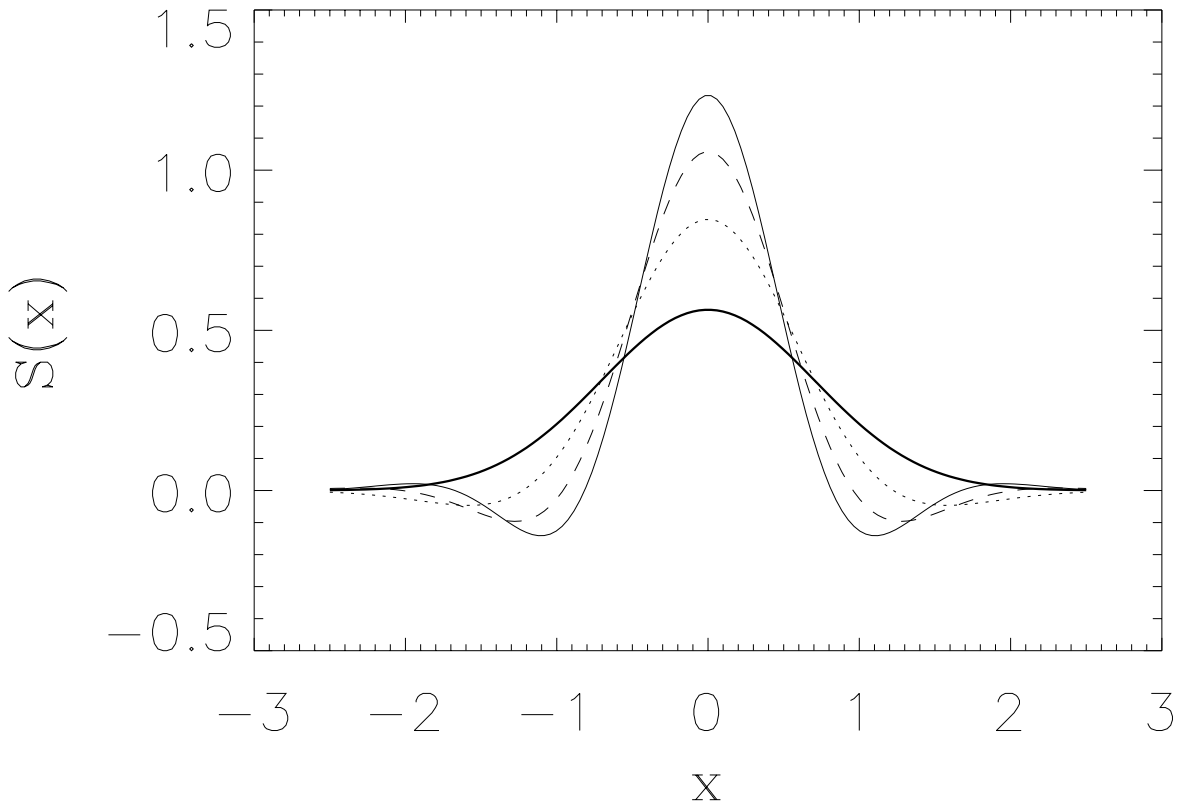

Figure 1: Gaussian-based shape functions with infinite support of order 0 (thick plain line), order 1 (dotted line), order 2 (dashed line) and order 3 (thin plain line).

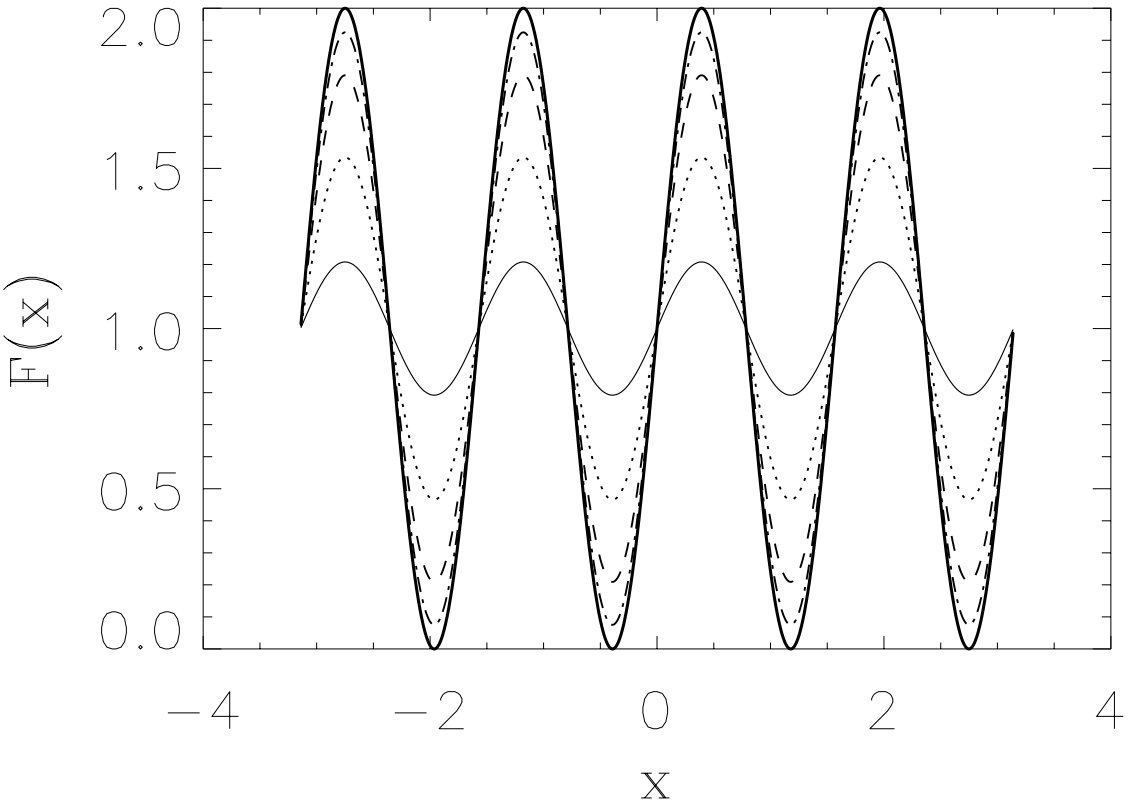

Figure 2: Exact (thick plain line) and approximate representations of the test function $\phi_M(x) = 1 + \sin(M\pi x/L)$ with $L = \pi$ and mode number $M = 4$ for a set of $N = 32$ uniformly distributed markers. The approximate representations shown as a thin plain line, a dotted line, a dashed line and a dotted-dashed line are for shape functions with smoothness order 0,1,2 and 3, respectively.

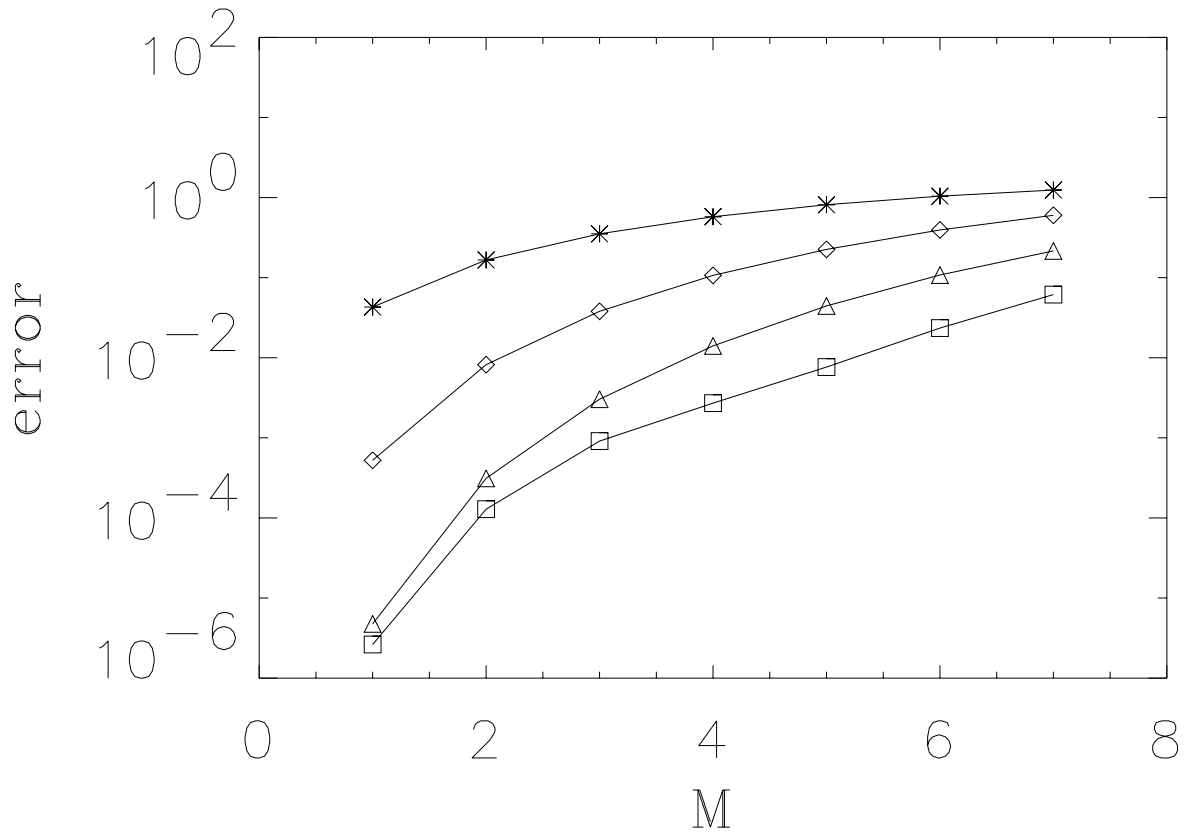

Figure 3: L^2 norm of the error for the test function $\phi_M(x) = 1 + \sin(M\pi x/L)$ as a function of the mode number M for shapes function with smoothness order 0 (asterisks), 1 (diamonds), 2 (triangles) and 3 (squares)

.

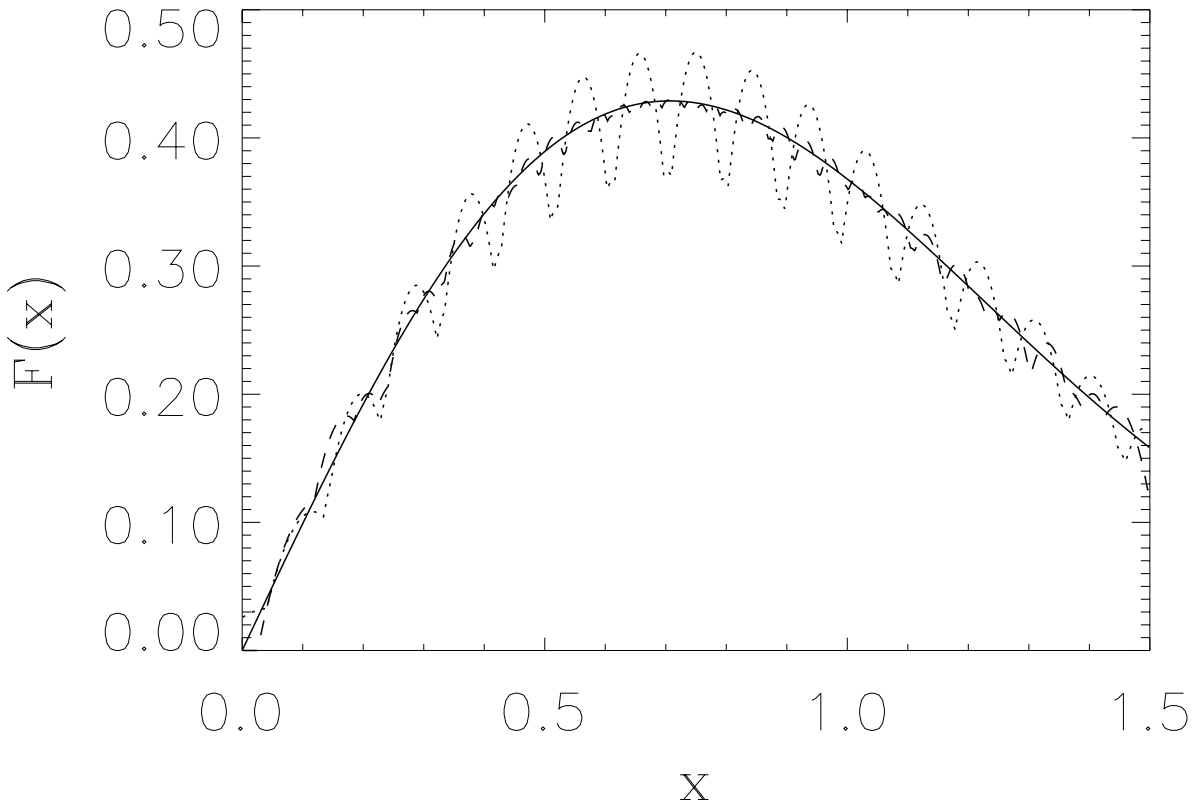

Figure 4: Approximation of the function $f(x) = xe^{-x^2}$ (plain line) based on a set of $N = 32$ markers. The dotted (dashed) line is for the case of uniform (nonuniform) spatial loading. The shape function is a quadratic polynomial [$S(x) = S_3(x)$; see Eq.(11)] with parameter $\epsilon = 0.1$.

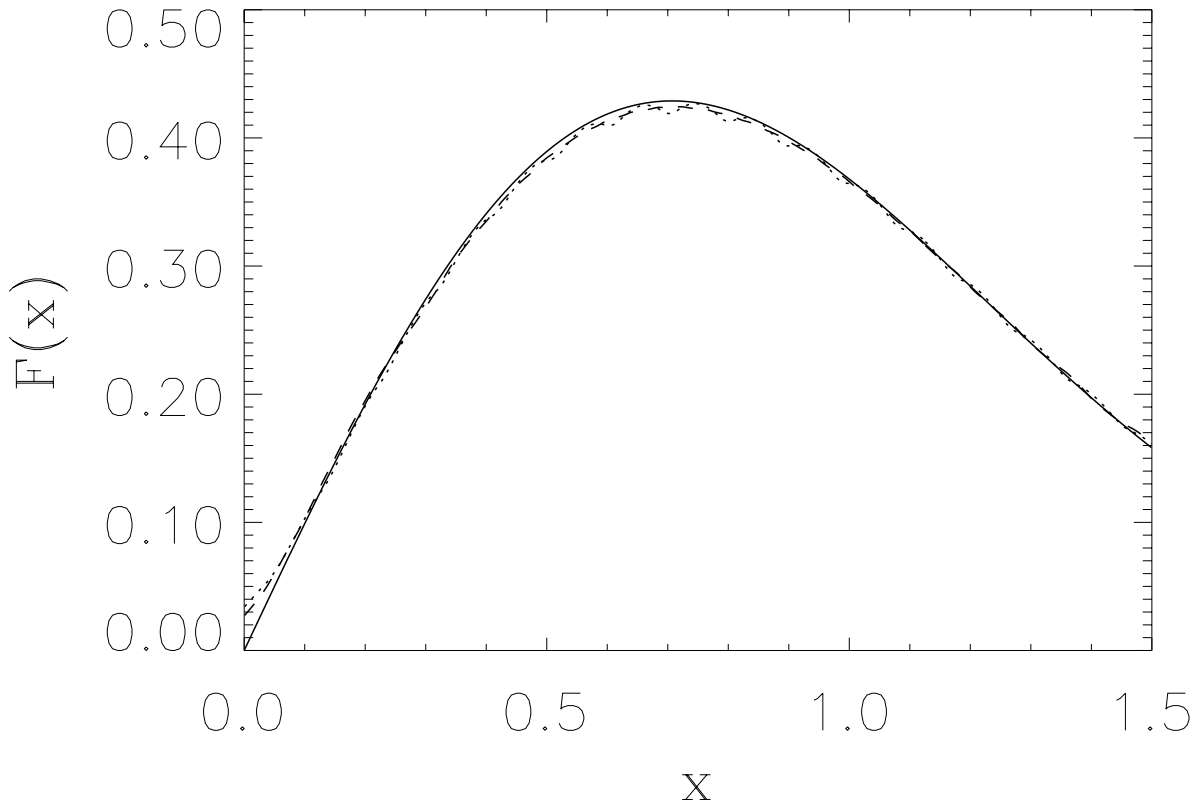

Figure 5: Approximation of the function $f(x) = xe^{-x^2}$ (plain line) based on a set of $N = 32$ markers. The dotted (dashed) line is for the case of uniform (nonuniform) spatial loading. The shape function is a quartic polynomial $[S(x) = S_4(x)$; see Eq.(11)] with parameter $\epsilon = 0.2$.

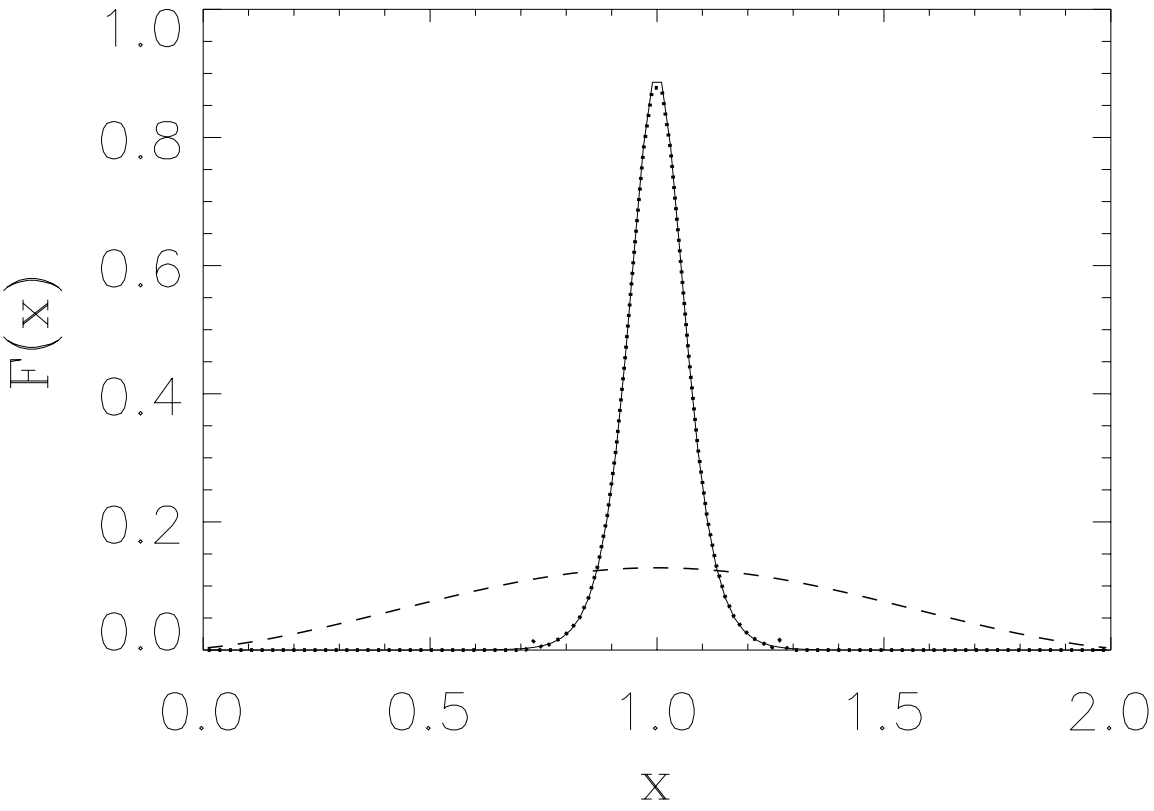

Figure 6: Approximated profiles (dashed line: $\epsilon = 1$; dotted line: $\epsilon = \epsilon_{\rm opt}$) for the function $f(x)$ given by Eq.(21) (thin plain line). The parameters are: $N = 400$, $N_g = 100$ and $\Delta\tau = 0.05$.

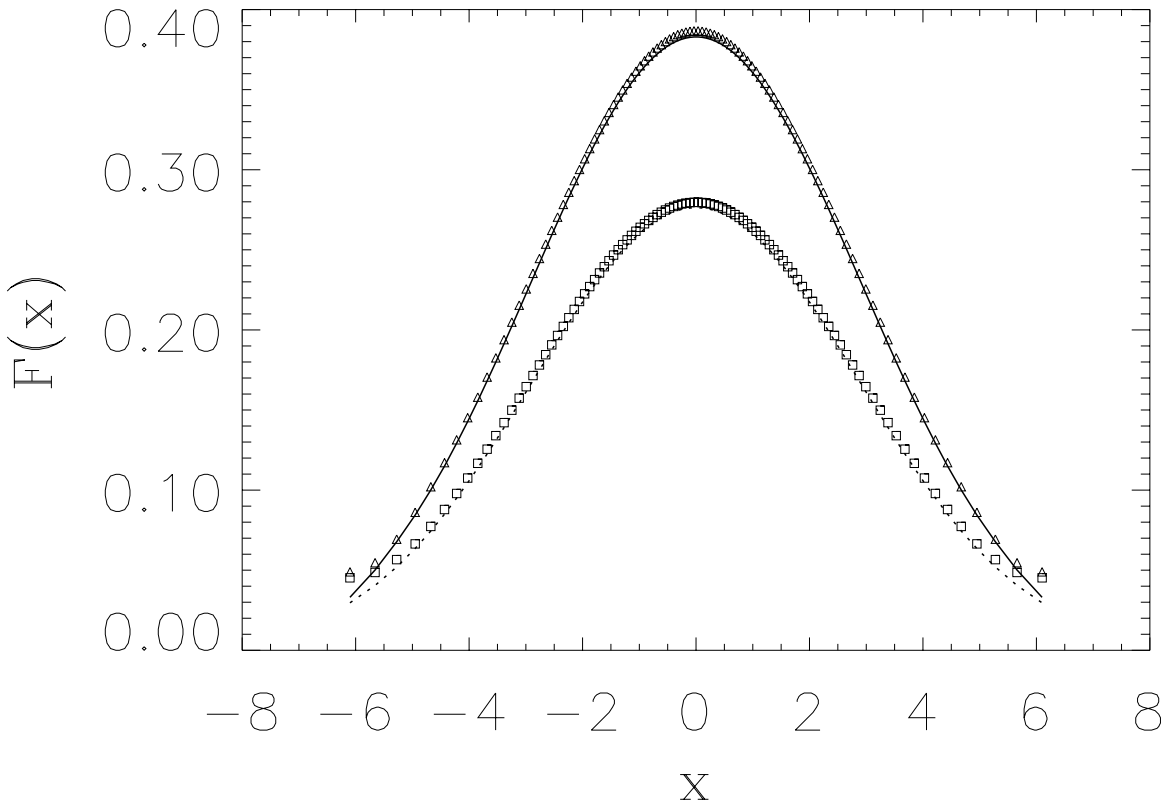

Figure 7: Exact (plain line: $t = 2.0$; dotted line: $t = 4.0$) and approximate (triangles: $t = 2.0$; squares: $t = 4.0$)) solutions of the diffusion equation based on a set of $N = 100$ markers. The initial condition is a square profile, Eq.(22). The shape function is a superGaussian [Eq.(23)]. Other parameters are: $\Delta t = 0.01$, $\epsilon = 1/3$ and $L = 14.0$.

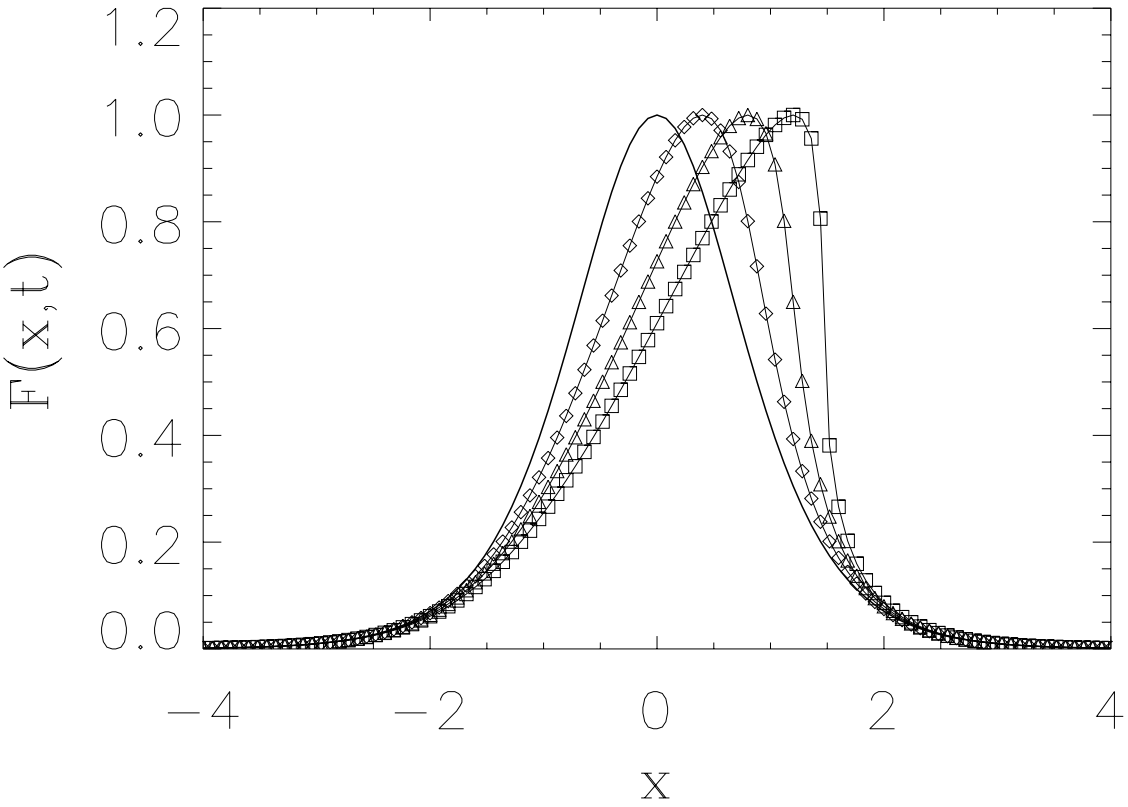

Figure 8: Exact (thin plain lines) and approximate (diamonds: $t = 0.4$, triangles: $t = 0.8$ and squares: $t = 1.2$) solution of the quasilinear equation $\partial f/\partial t + f\partial f/\partial x = 0$ with initial condition $f(x, 0) = \mathrm{sech}^2 x$ (thick plain line). The number of markers is $N = 128$, the time step is $\Delta t = 0.001$ and the support parameter is $\epsilon = \sqrt{h}$.

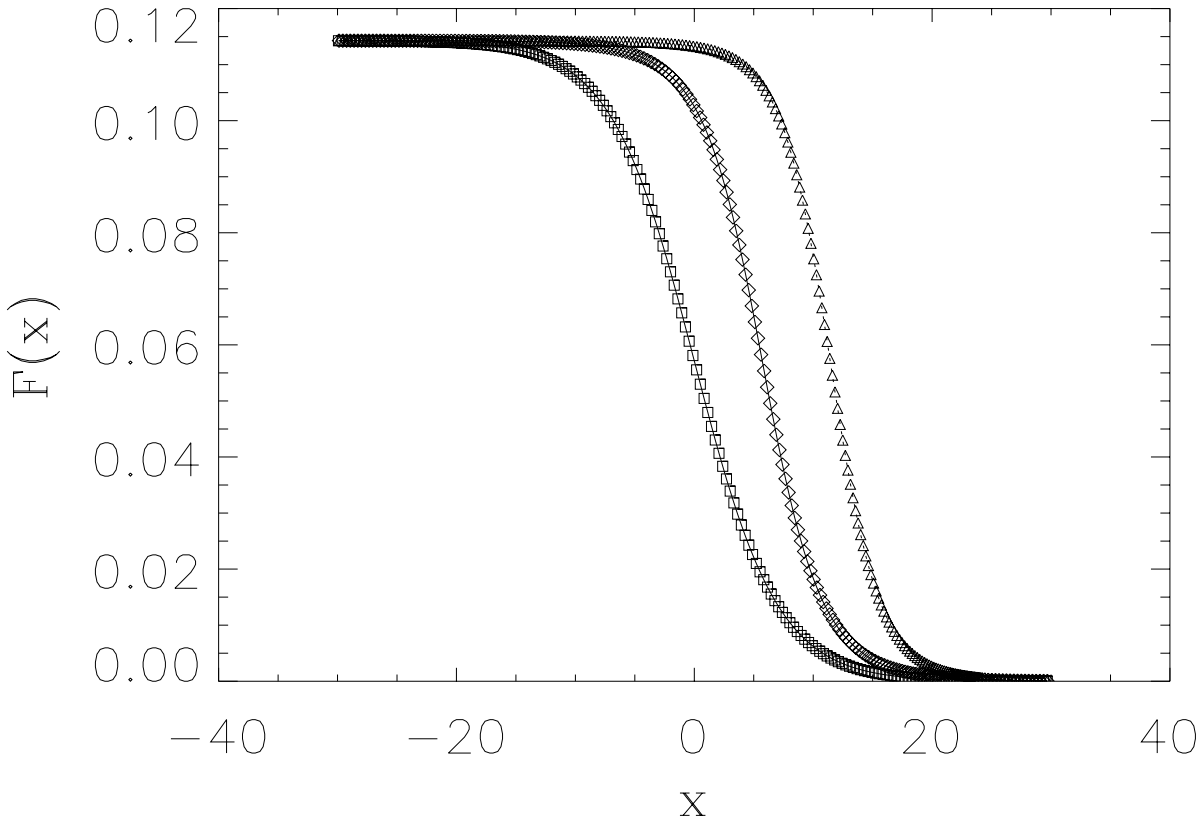

Figure 9: Exact (thin plain lines) and approximate (squares: $t = 0.0$, diamonds: $t = 100$ and triangles: $t = 200$) solution of the nonlinear Burgers equation with initial conditions given by Eq.(27). The parameters are: $\mu = 0.1$, $\lambda = 7.0$ and $A = 4.0$. The number of markers used is $N = 256$ and the time step of integration is $\Delta t = 0.1$.

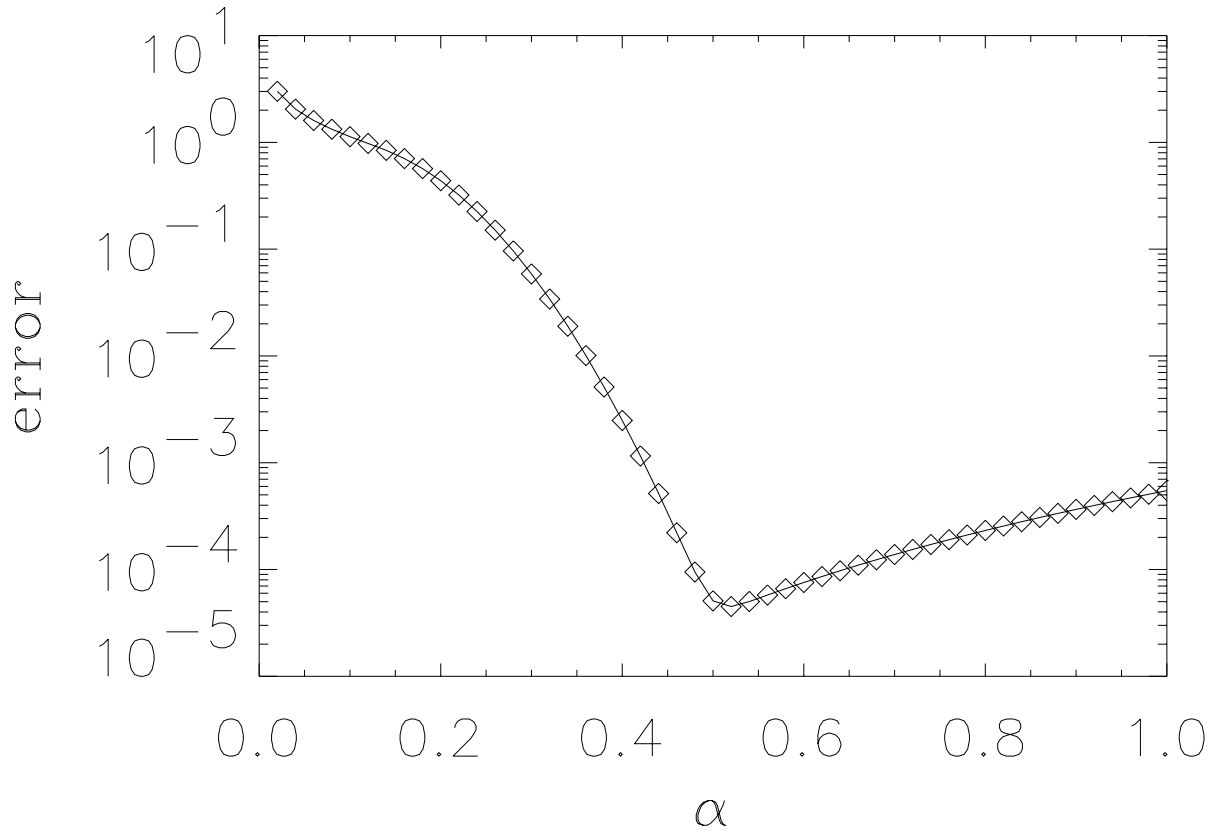

Figure 10: L^2 norm of the error determined on a fixed grid with $N_g = 5000$ grid points as a function of α for the profile $F_0(x) = \mathrm{sech}^2(x/2)/2$ and a set of $N = 128$ markers. The parameter α is related to the support parameter through the relation $\epsilon = \alpha\sqrt{h}$. The markers are distributed uniformly in the interval $x \in [-L, L]$ with $L = 12$ and $h = 2L/N = 3/16$.

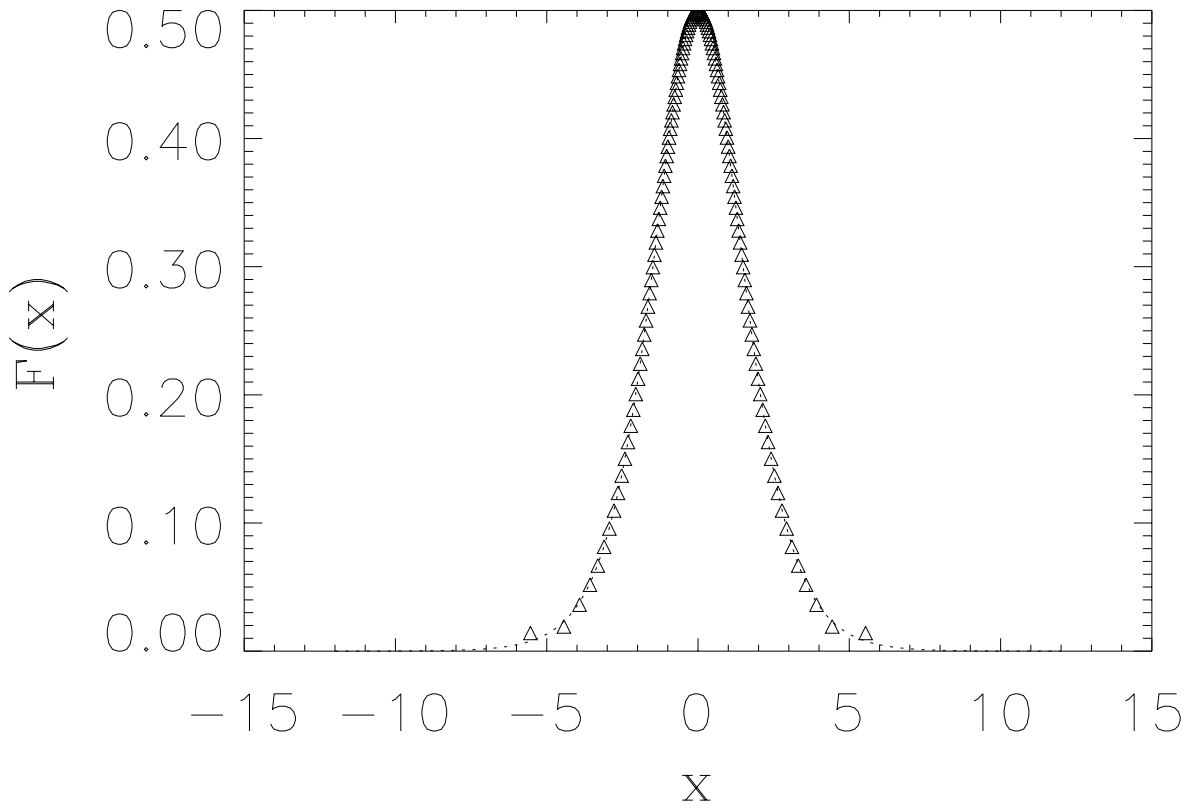

Figure 11: Initial profile $F_0(x) = \mathrm{sech}^2(x/2)/2$ based on a set of $N = 128$ markers with uniform weights distributed in the interval $x \in [-12, 12]$. The triangles denote the positions of the markers whereas the dotted line is the exact profile.

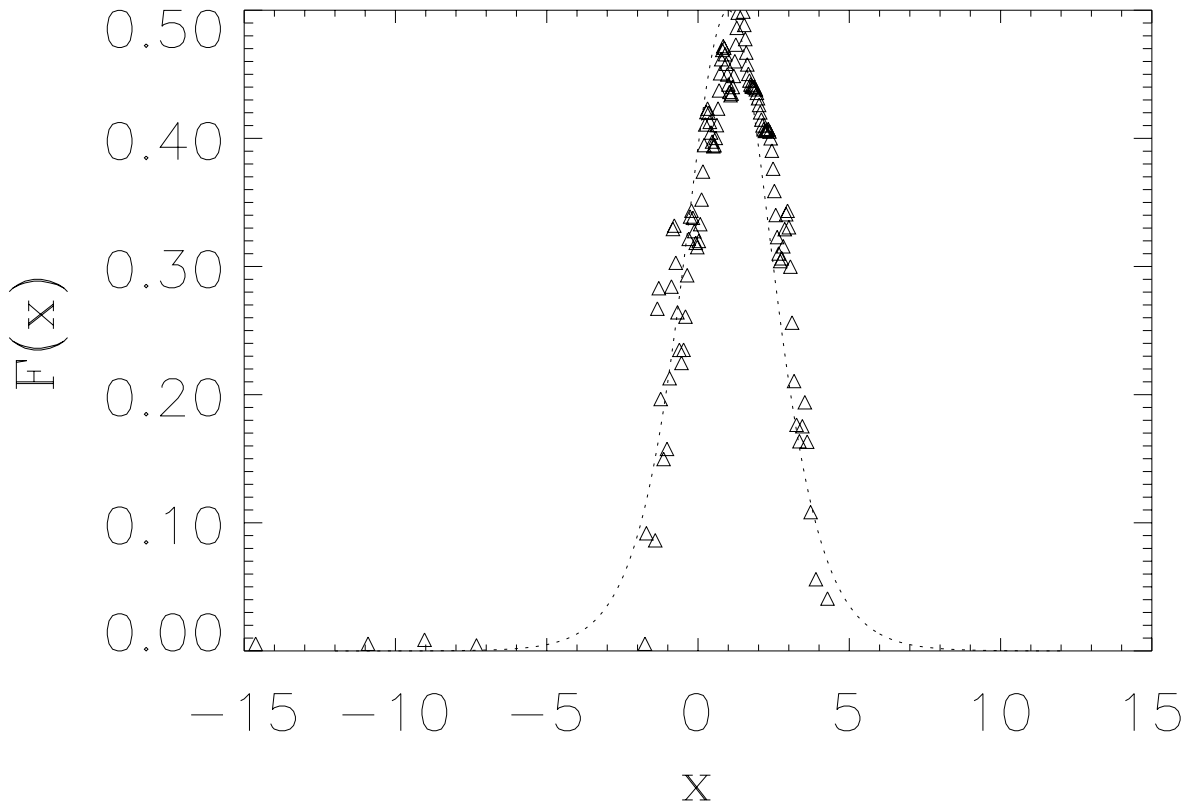

Figure 12: Single soliton at $t = 0.1$ with initial profile $F_0(x) = \mathrm{sech}^2(x/2)/2$. The shape function used is a superGaussian of smoothness order 1 (infinite support). At $t = 0$ the markers were loaded as in Fig.11. The time step used is $\Delta t = 0.002$. The triangles represent the position of the markers and the exact profile is shown as a dotted line.

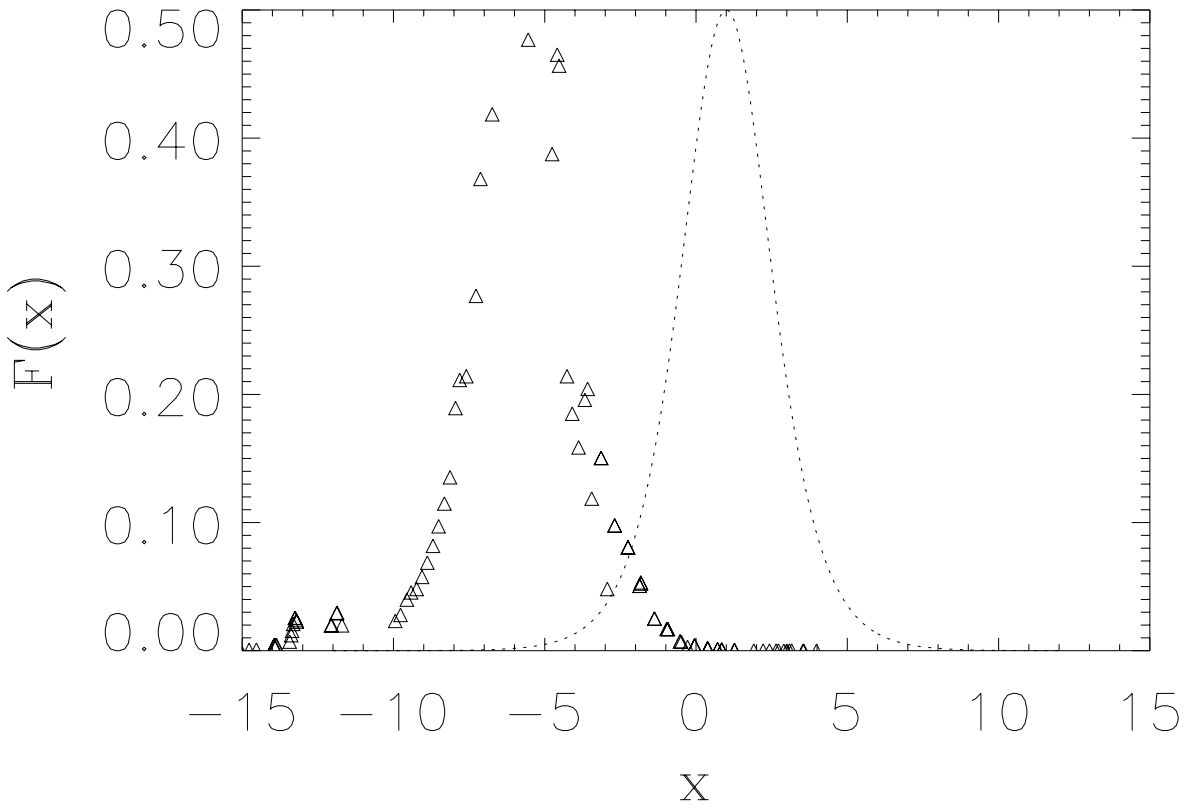

Figure 13: Same as Fig.12 but for the case of a shape function with finite support based on a quadratic polynomial/Gaussian profile.

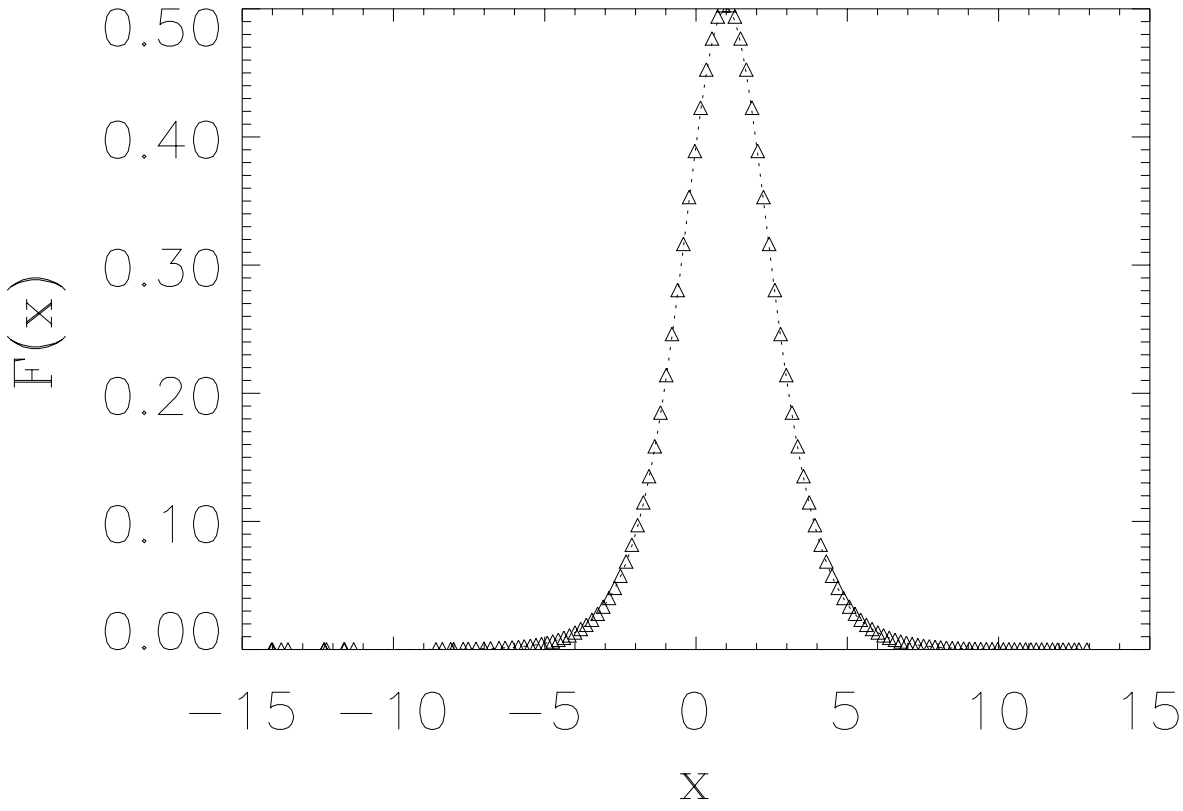

Figure 14: Same as Fig.12 for the case of nonuniform weights.

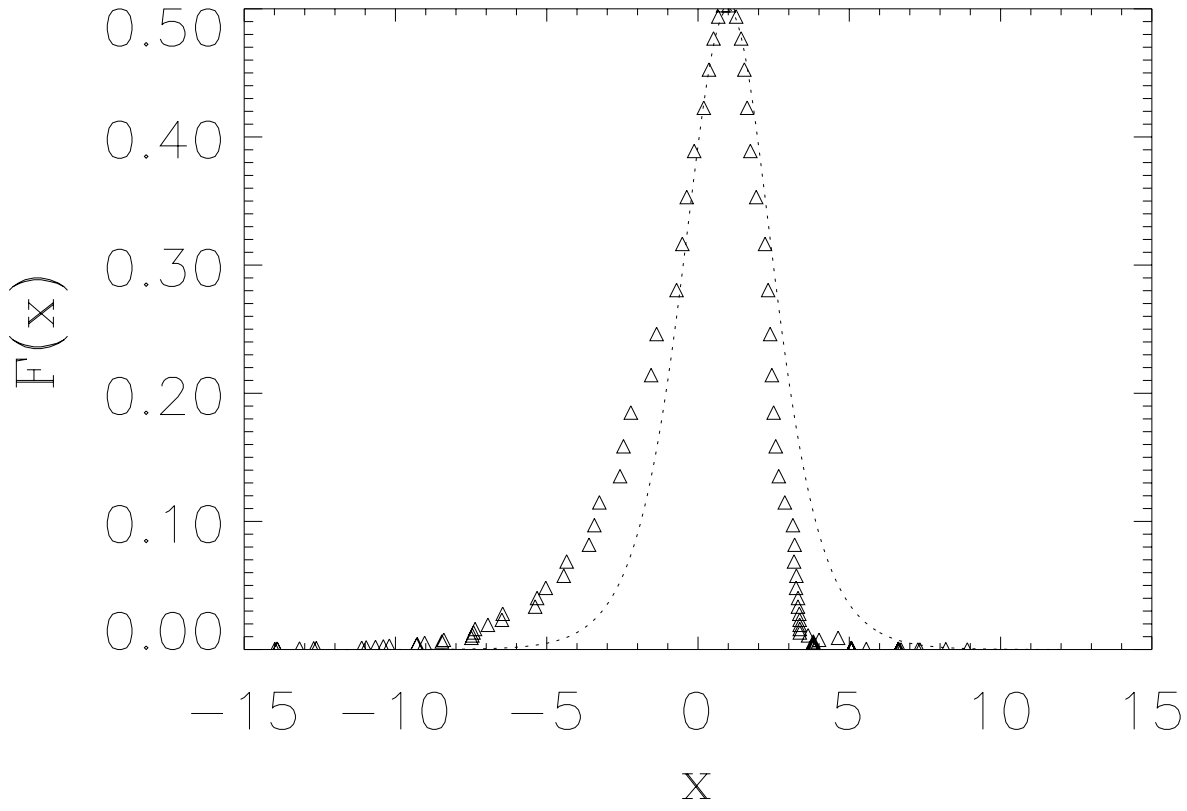

Figure 15: Same as Fig.14 but for a larger time step of $\Delta t = 0.01$.

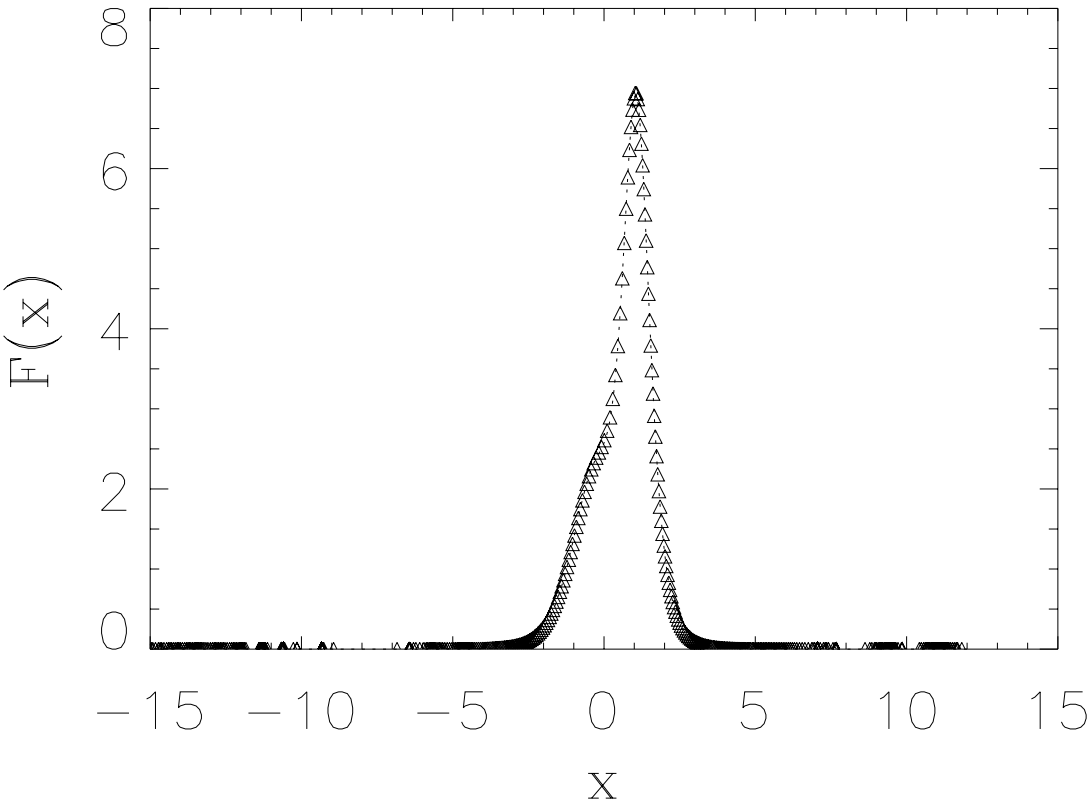

Figure 16: Double soliton at $t = 0.05$ with initial profile $F_0(x) = 6\text{sech}^2(x)$ for a set of $N = 500$ markers in the interval $x \in [-15, 12]$. The time step used is $\Delta t = 1.0 \times 10^{-5}$, the shape function is a superGaussian of smoothness order 1 and the support parameter is $\epsilon = \sqrt{h}$.

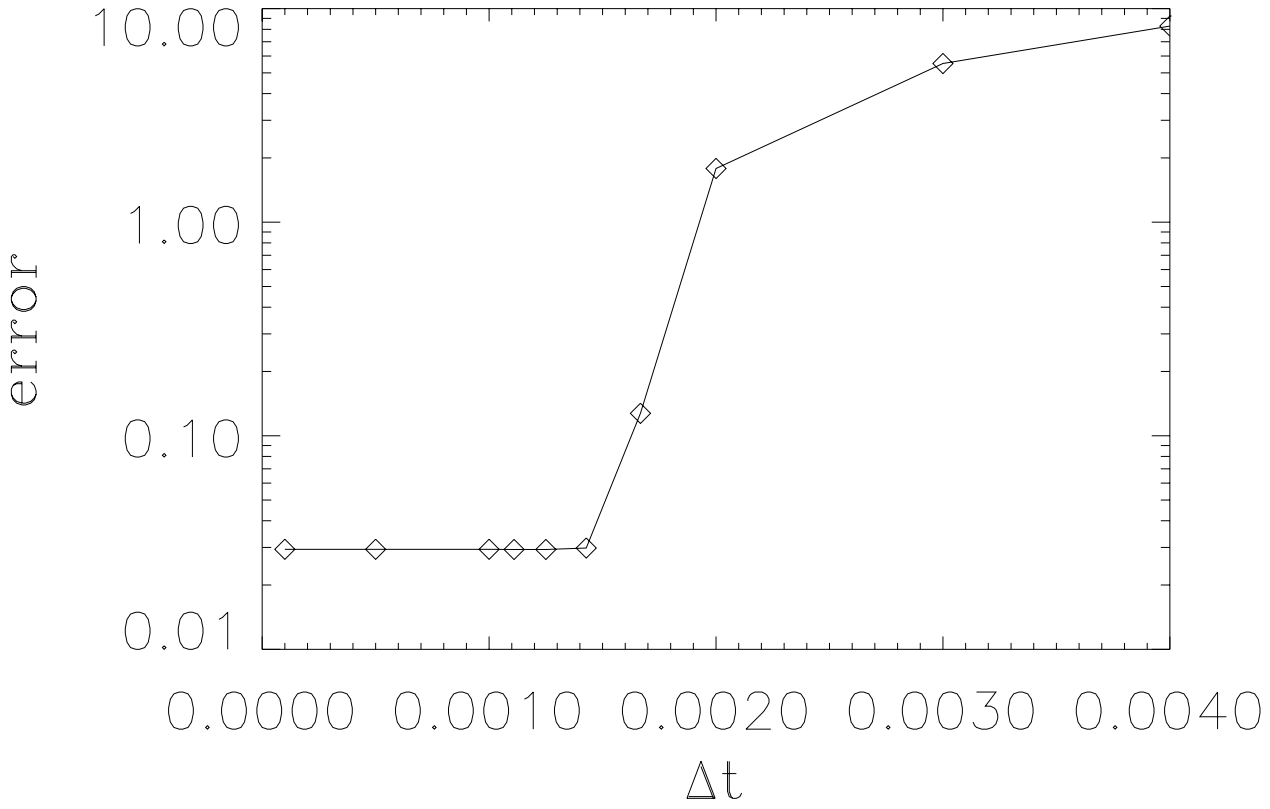

Figure 17: L^2 norm of the error at $t = 0.1$ for the double soliton case as a function of the time step of integration. All the parameters are the same as in Fig.16.

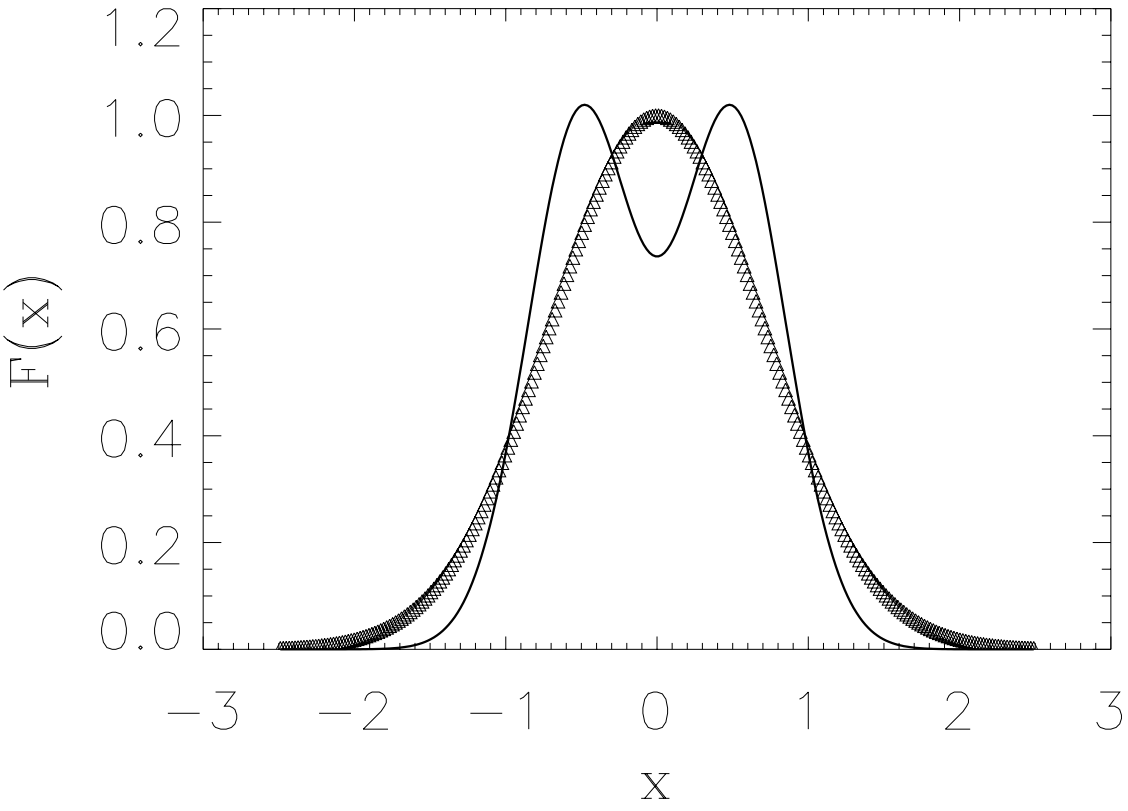

Figure 18: Steady state solution of the one-dimensional nonlinear diffusion equation (35) (plain line). The triangles represents the initial position of the markers.

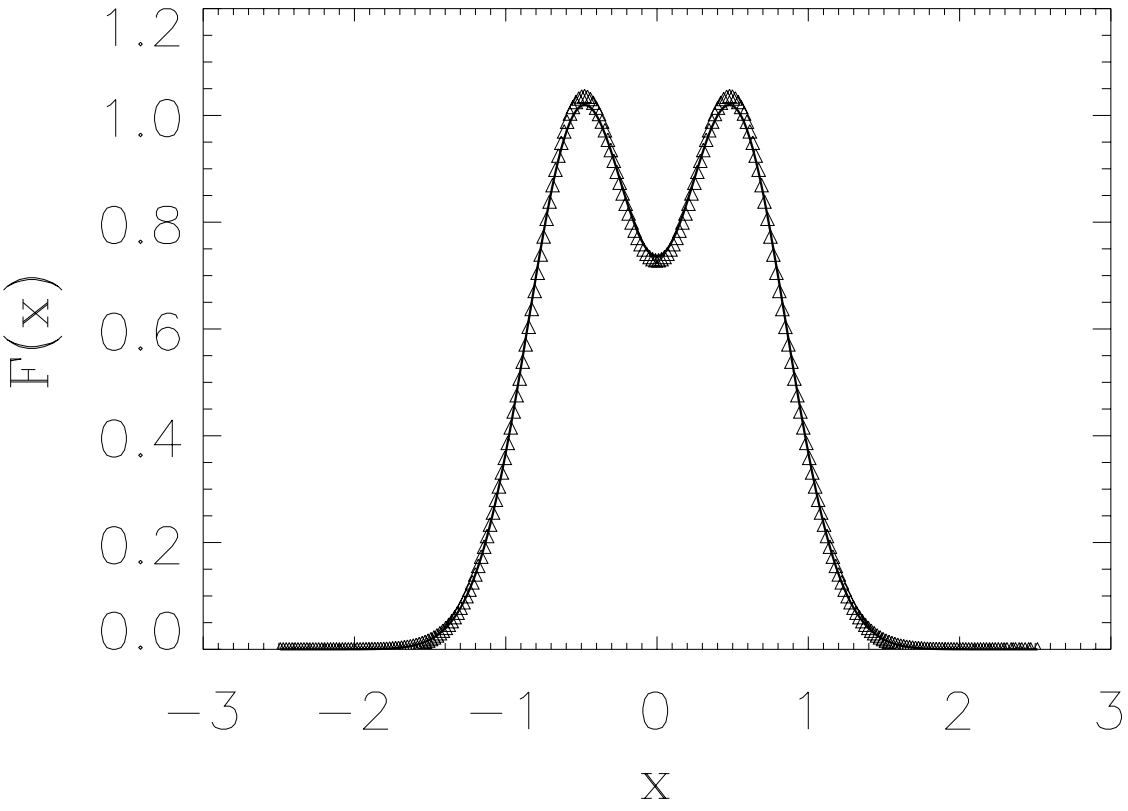

Figure 19: Steady state solution of the one-dimensional nonlinear diffusion equation (35) (plain line). The triangles represents the position of the markers at $t = 80$.

External Distribution

Plasma Research Laboratory, Australian National University, Australia

Professor I.R. Jones, Flinders University, Australia

Professor João Canalle, Instituto de Fisica DEQ/IF - UERJ, Brazil

Mr. Gerson O. Ludwig, Instituto Nacional de Pesquisas, Brazil

Dr. P.H. Sakanaka, Instituto Fisica, Brazil

The Librarian, Culham Science Center, England

Mrs. S.A. Hutchinson, JET Library, England

Professor M.N. Bussac, Ecole Polytechnique, France

Librarian, Max-Planck-Institut für Plasmaphysik, Germany

Jolan Moldvai, Reports Library, Hungarian Academy of Sciences, Central Research Institute for Physics, Hungary

Dr. P. Kaw, Institute for Plasma Research, India

Ms. P.J. Pathak, Librarian, Institute for Plasma Research, India

Professor Sami Cuperman, Plasma Physics Group, Tel Aviv University, Israel

Ms. Clelia De Palo, Associazione EURATOM-ENEA, Italy

Dr. G. Grosso, Instituto di Fisica del Plasma, Italy

Librarian, Naka Fusion Research Establishment, JAERI, Japan

Library, Laboratory for Complex Energy Processes, Institute for Advanced Study, Kyoto University, Japan

Research Information Center, National Institute for Fusion Science, Japan

Dr. O. Mitarai, Kyushu Tokai University, Japan

Dr. Jiangang Li, Institute of Plasma Physics, Chinese Academy of Sciences, People's Republic of China

Professor Yuping Huo, School of Physical Science and Technology, People's Republic of China

Library, Academia Sinica, Institute of Plasma Physics, People's Republic of China

Librarian, Institute of Physics, Chinese Academy of Sciences, People's Republic of China

Dr. S. Mirnov, TRINITI, Troitsk, Russian Federation, Russia

Dr. V.S. Strelkov, Kurchatov Institute, Russian Federation, Russia

Professor Peter Lukac, Katedra Fyziky Plazmy MFF UK, Mlynska dolina F-2, Komenskeho Univerzita, SK-842 15 Bratislava, Slovakia

Dr. G.S. Lee, Korea Basic Science Institute, South Korea

Dr. Rasulkhozha S. Sharafiddinov, Theoretical Physics Division, Insitute of Nuclear Physics, Uzbekistan

Institute for Plasma Research, University of Maryland, USA

Librarian, Fusion Energy Division, Oak Ridge National Laboratory, USA

Librarian, Institute of Fusion Studies, University of Texas, USA

Librarian, Magnetic Fusion Program, Lawrence Livermore National Laboratory, USA

Library, General Atomics, USA

Plasma Physics Group, Fusion Energy Research Program, University of California at San Diego, USA

Plasma Physics Library, Columbia University, USA

Alkesh Punjabi, Center for Fusion Research and Training, Hampton University, USA

Dr. W.M. Stacey, Fusion Research Center, Georgia Institute of Technology, USA

Dr. John Willis, U.S. Department of Energy, Office of Fusion Energy Sciences, USA

Mr. Paul H. Wright, Indianapolis, Indiana, USA

The Princeton Plasma Physics Laboratory is operated
by Princeton University under contract
with the U.S. Department of Energy.

Information Services
Princeton Plasma Physics Laboratory
P.O. Box 451
Princeton, NJ 08543

Phone: 609-243-2750
Fax: 609-243-2751
e-mail: pppl_info@pppl.gov
Internet Address: http://www.pppl.gov